Review Article

INTERNATIONAL JOURNAL OF ADVANCED ROBOTIC SYSTEMS

International Journal of Advanced Robotic Systems
September-October 2016: 1–25

DOI: 10.1177/1729881416662537
arx.sagepub.com
SAGE

Experimental evaluation of acceleration waveform replication on electrohydraulic shaking tables: A review

Gang Shen[1,2], Zhencai Zhu[1,2], Xiang Li[1,2], Ge Li[1,2], Yu Tang[1,2], and Shanzeng Liu[1]

Abstract

An electrohydraulic shaking table is an essential experimental facility in many industrial applications to real-time simulate actual vibration situations including structural vibration and earthquake. However, there is still a challenging area for its acceleration waveform replication because acceleration output responses of the electrohydraulic shaking table would not be as intended in magnitude and phase of an acceleration closed-loop system due to inherent hydraulic nonlinear dynamics of electrohydraulic servo systems. Thus, how to accurately and coordinately control parallel hydraulic actuators of the electrohydraulic shaking table is a critical issue; so, many control techniques have been developed to address the issue. Some currently used key techniques in this field are reviewed in the article, which are the objectives of academic investigations and industrial applications. The article reviews some new control algorithms for the electrohydraulic shaking table to obtain high-fidelity acceleration waveform replication accuracy.

Keywords

Electrohydraulic shaking table, parallel redundant mechanism, feed-forward inverse model compensation control, adaptive control, off-line iterative control, three-variable control, system identification

Date received: 5 May 2016; accepted: 14 July 2016

Topic: Special Issue - Manipulators and Mobile Robots
Topic Editor: Tomas Brezina

Introduction

An electrohydraulic shaking table (EHST) is an important experimental testing tool to replicate actual vibration situations for evaluating original structural performances of a tested specimen in civil and architectural engineering,[1–5] automotive industry,[6,7] earthquake resistance testing,[8–12] structure fatigue testing,[13–15] and so on. Due to potential advantages of the EHST in power density, large forces, high-fidelity position and acceleration tracking accuracy,[16–19] high durability and stiffness, a rapid and wide frequency output response, and more accurate vibration tests, many investigations have been carried on their academic studies and industrial applications.[2,20]

However, dynamic characteristics of acceleration output responses on the EHST would not be intended in its magnitude and phase[21,22] due to inherent nonlinearities and uncertainties of the EHST, such as dynamics of servovalves and hydraulic actuators.[17,23–26] Besides, disturbed reaction forces generated by a specimen deteriorate,[27,28] dynamics of the base support,[29] and internal coupling force in the EHST,[16,17,22] and so on, affect acceleration tracking control performances. Many compensation approaches for

[1] School of Mechatronic Engineering, China University of Mining and Technology, Xuzhou, China
[2] Jiangsu Key Laboratory of Mine Mechanical and Electrical Equipment, China University of Mining and Technology, Xuzhou, China

Corresponding author:
Zhencai Zhu, China University of Mining and Technology, #1 Daxue Road, Xuzhou 221116, China.
Email: zhuzhencai@vip.163.com

acceleration waveform replication on the EHST have been employed to minimize nonlinear behaviors of electrohydraulic servo systems, such as off-line feed-forward compensation controllers including a three-variable controller (TVC),[2,18–20,30–36] a feed-forward inverse model controller (FIMC),[2,18,19,22,34–39] and an off-line iterative controller (OIC)[2,20,34,36,40–44] and online adaptive controllers including adaptive inverse control (AIC),[18,21,22,33,35,37,44–48] minimal control synthesis (MCS),[2,18,37,39,40,49–53] an adaptive notch filter compensator (ANFC),[27,28] amplitude phase control (APC),[20,32] adaptive harmonic cancellation (AHC),[54–56] and so on. Control technologies used for general electrohydraulic servo systems have been reviewed by Plummer[2] and Yao et al.[20] With such a vast array of compensation algorithms, it became difficult to determine which controllers to be employed for the EHST practical applications. The aim of the review article is to provide an overview of main experimental results obtained with different control approaches for the benefit of the person responsible. The article focuses on control technologies that are most often used or most promising technologies for acceleration waveform replication on the EHST, as well as recent academic studies, but inevitably, these technologies are far from being comprehensive. Figure 1 summarizes some main controllers for acceleration waveform replication on the EHST.

The goal of this article is to review control technologies for the EHST to improve control performances of the acceleration waveform replication. To develop the idea, a dynamic model of the EHST is established to verify the effectiveness of these controllers for simulation. A coordinate controller as a basic controller is employed to operate a redundant EHST. These off-line compensation controllers including the TVC, the FIMC, and the OIC are employed to expand the frequency bandwidth of the acceleration closed-loop system and obtain an asymptotic performance of the acceleration waveform replication. In order to obtain a better acceleration waveform replication accuracy on the EHST, online adaptive controllers and their combined controllers are employed to further adaptively adjust time domain drive signals. The effectiveness of reviewed controllers is examined by some experiments on an experimental redundant EHST with six degree of freedoms (six-DOFs) controlled by eight hydraulic actuators and servo-valves. To evaluate advantages and drawbacks of these reviewed controllers, comparison of relative controllers and their evaluation analysis are presented and main conclusions are summarized.

According to controllers used in the EHST, as shown Figure 1, contribution is organized as follows: "Dynamic model of the EHST" section describes a structural and mathematical model of the EHST, respectively. A coordinate controller for the redundant EHST is reviewed in section "Coordinate controller." "Three-variable controller" section concerns with the TVC to improve stability and the frequency bandwidth of the acceleration closed-loop system of the EHST. "Feed-forward inverse model controller" section reviews transfer function

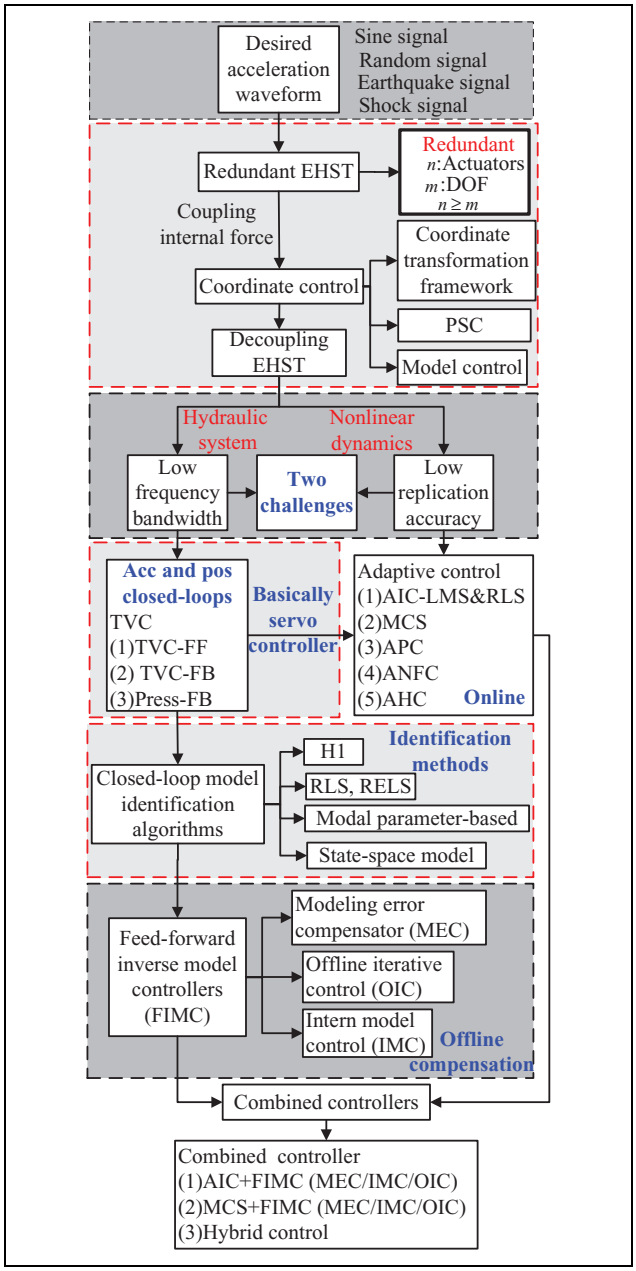

Figure 1. Control technologies for the EHST. EHST: electrohydraulic shaking table.

identification methods, feed-forward inverse model design methods, and the FIMC and its improved control schemes with modeling error compensators. "Off-line iterative controller" section reviews OICs. "Online adaptive controller" section reviews adaptive controllers and their combined controllers based on adaptive control and off-line compensators are reviewed in section "Combined controller." To evaluate advantages and drawbacks of different controllers, simulation comparison of reviewed controllers and their evaluation analysis are presented in section "Simulation evaluation analysis of main reviewed controllers." An experimental setup of the redundant EHST is employed in section "Experimental setup of the EHST" to verify the effectiveness of reviewed

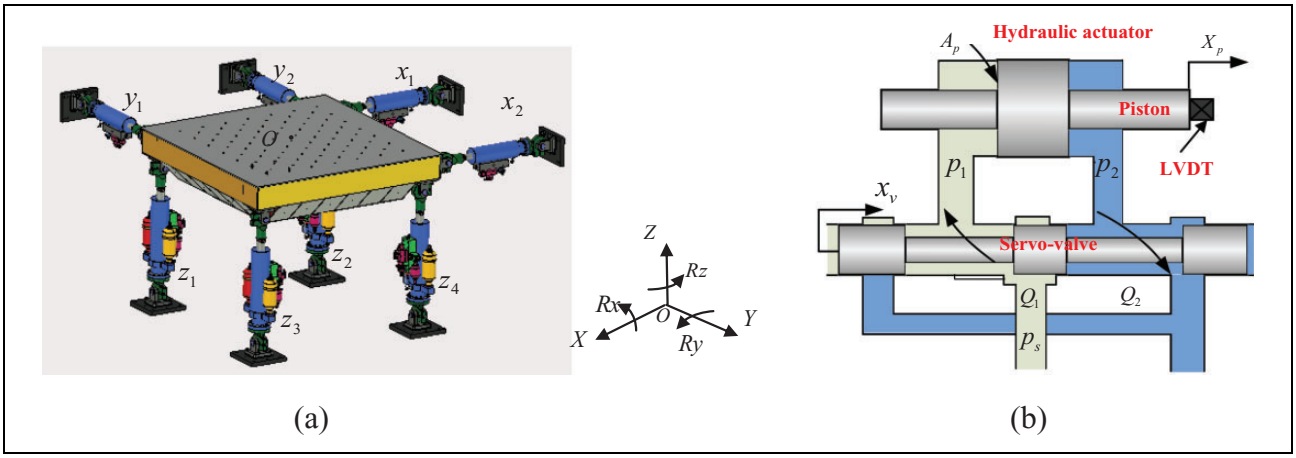

Figure 2. Classical configuration (a) of a redundant EHST and (b) its simplified working principle of one actuator. EHST: electrohydraulic shaking table.

controllers. Some experiments are performed in section "Experimental evaluation analysis of main reviewed controllers," and experimental results verify acceleration waveform replication performances of reviewed controllers. The main conclusions are summarized in "Concluding remarks" section.

Dynamic model of the EHST

A structure of an experimental EHST is shown in Figure 2(a), which is a six-DOF parallel redundant mechanism, including X, Y, and Z translations, and roll R_x, pitch R_y, and yaw R_z, using eight hydraulic servo units that are composed of eight servo-controlled hydraulic actuators and eight servo-valves. A single hydraulic actuator configuration of the EHST is established in Figure 2(b) because dynamic responses of each actuator are similar, where A_p is the effective area of the hydraulic actuator, Q_1 is flow into the chamber, and Q_2 is flow out of the chamber of the hydraulic cylinder, x_p is the piston displacement measured by a linear variable differential transformer (LVDT), x_v is the spool displacement of the servo-valve, p_1 and p_2 are pressures in the two chambers, and p_s is the hydraulic supply pressure. A simplified open-loop dynamic model of the EHST system is established,[19] which is given by

$$G_{op}(s) = \frac{K_0}{s\left(\frac{s^2}{\omega_{sv}^2} + \frac{2\xi_{sv}}{\omega_{sv}}s + 1\right)\left(\frac{s^2}{\omega_h^2} + \frac{2\xi_h}{\omega_h}s + 1\right)} \quad (1)$$

where K_0 is the open-loop gain of the EHST, defined by $K_0 = K_{sv}K_q/A_p$, in which K_{sv} is a servo-valve gain, K_q is the linearized flow gain; ω_h and ξ_h are the hydraulic natural frequency and the damping ratio of the actuator, respectively, which are defined by $\omega_h = \sqrt{4\beta_e A_p^2/m_t V_t}$ and $\xi_h = ((K_c + C_{tp})/A_p)\sqrt{\beta_e m_t/V_t} + (B_c/4A_p)\sqrt{V_t/\beta_e m_t}$, in which β_e is the effective bulk modulus, m_t is the total mass of the actuator piston, load, and specimen, V_t is the total volume of the actuator, K_c is the flow pressure coefficient, C_{tp} is the total leakage coefficient of the actuator including an internal leakage coefficient C_{ip} and an external leakage coefficient C_{ep}, whose relation is given by $C_{tp} = C_{ip} + C_{ep}/2$, and B_c is the viscous damping coefficient between the piston and payload; ω_{sv} and ξ_{sv} are the natural angular frequency and the damping coefficient of the servo-valve, respectively.

A linear model that serves as a standard dynamic model of the EHST is employed in engineering applications. Various linearized models for the EHST have been employed to minimize the influence of nonlinearities for real-time testing,[17,19,26,27,53,57,58] and nonlinear models of electrohydraulic servo systems have attracted the attention of many researchers.[59–62] Duration nonlinearities of a servo-valve have been included in the literature.[59] Nonlinear characteristics of a dynamic model for a real-time full-scale seismic testing system have been noted in the literature.[60] Williams et al.[61] developed a realistic model of a dynamic structural testing system, which includes a nonlinear model of a servo-valve-controlled actuator system, the controller, and model of test specimen. Zhao et al.[62] proposed a nonlinear system model for the effective force testing system in which a detail nonlinear servo-valve model is employed. Plummer[26] described a detailed simulation model for a six-DOF shaking table including servo-valve response and structural effects, significant nonlinearities associated with the hydraulic and mechanical components.

A review with controllers of the EHST

Coordinate controller

A six-DOF redundant EHST with eight hydraulic actuators cannot work normally due to geometric effects,[16] different parameters, and installation errors of eight actuators, which may cause a large dynamic internal coupling force in the redundant EHST. A general transformation framework for multiaxis motion parallel actuator systems is presented in the literature.[16] An eight-DOF control method was employed to implement independent control of the

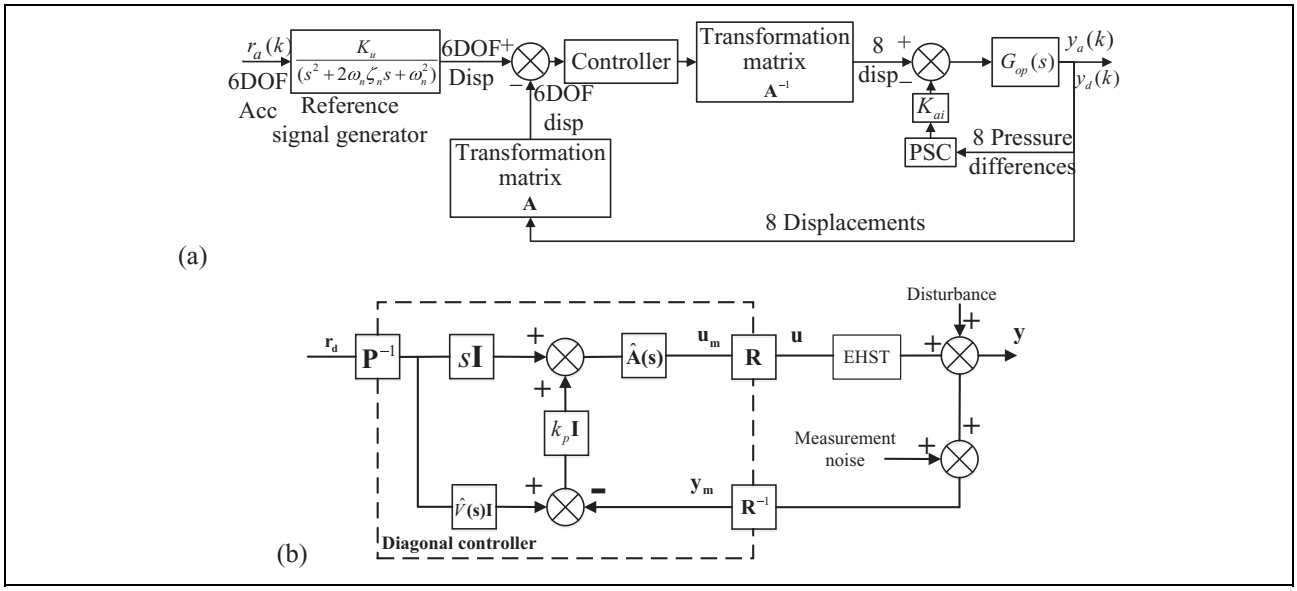

Figure 3. Coordinate controller of the redundant EHST: (a) coordinate controller based on the PSC and transform matrix and (b) a multiaxis decoupling controller.[17] EHST: electrohydraulic shaking table; PSC: pressure stabilizing controller.

EHST.[22] Some multiaxis random vibration control methods for the EHST have been presented.[63–66] Although the coordinate controller based on transformation matrixes can eliminate the statically indeterminate problem of the redundant EHST, an internal coupling force due to each parameter inconformity and installation errors among eight actuators cannot be avoided. A pressure stabilizing controller (PSC) is designed to reduce the internal coupling force. A redundant force controller is developed to reduce the cross-coupling among actuators.[67] Recently, a multiaxis modal controller and a dynamic compensator are new methods that have been applied to the redundant EHST to decouple the internal coupling force.[17,68,69] Plummer[17] presented a new model-based motion control method for multiaxis EHSTs, and ability of this method to decouple control axes is demonstrated. A modal space control approach for a hydraulically driven fully parallel mechanism with actuation redundancy is described in the literature,[68] and zero-eigenvalue modes are equivalent to the modulation of internal forces for reducing the internal coupling force in the redundant parallel mechanism. A modal analysis method is employed to clearly analyze dynamic coupling characteristics of a spatial six-DOF parallel manipulator, the dynamic coupling evaluation matrix is used to reflect the coupling relationship, and the coupling strength is defined in the literature.[69] A coordinate controller of the six-DOF-controlled EHST is designed, as shown in Figure 3, where $r_a(k)$, $y_d(k)$, and $y_a(k)$ are the acceleration reference signal, the actual position, and acceleration feedback signals, respectively; K_{ai} are gains of the PSC, in which i represents hydraulic actuators; an acceleration signal generator with a second-order filter $K_u/(s^2 + 2\omega_n\zeta_n s + \omega_n^2)$ is employed to transform a reference acceleration signal to a desired displacement drive signal of the hydraulic actuator for the position closed-loop, in which K_u is a reference signal generator gain; ξ_n and ω_n are the damping ratio and the original frequency of the acceleration control, respectively. Two transform matrixes by transforming eight channel feedback signals and six-DOF control signals are given by[16,22]

$$A = \begin{bmatrix} 0.5 & 0.5 & 0 & 0 & 0 & 0 & 0 & 0 \\ 0 & 0 & 0.5 & 0.5 & 0 & 0 & 0 & 0 \\ 0.25 & -0.25 & 0.25 & -0.25 & 0 & 0 & 0 & 0 \\ 0.25 & -0.25 & -0.25 & 0.25 & 0 & 0 & 0 & 0 \\ 0 & 0 & 0 & 0 & 0.25 & 0.25 & 0.25 & 0.25 \\ 0 & 0 & 0 & 0 & 0.25 & 0.25 & -0.25 & -0.25 \\ 0 & 0 & 0 & 0 & 0.25 & -0.25 & 0.25 & -0.25 \\ 0 & 0 & 0 & 0 & 0.25 & -0.25 & -0.25 & 0.25 \end{bmatrix} \quad (2)$$

$$A^{-1} = \begin{bmatrix} 1 & 0 & 1 & 1 & 0 & 0 & 0 & 0 \\ 1 & 0 & -1 & -1 & 0 & 0 & 0 & 0 \\ 0 & 1 & 1 & -1 & 0 & 0 & 0 & 0 \\ 0 & 1 & -1 & 1 & 0 & 0 & 0 & 0 \\ 0 & 0 & 0 & 0 & 1 & 1 & 1 & 1 \\ 0 & 0 & 0 & 0 & 1 & 1 & -1 & -1 \\ 0 & 0 & 0 & 0 & 1 & -1 & 1 & -1 \\ 0 & 0 & 0 & 0 & 1 & -1 & -1 & 1 \end{bmatrix} \quad (3)$$

A complete multiaxis decoupling controller was proposed by Plummer in the literature,[17] which is shown in Figure 3(b), in which $\hat{A}(s)$ is an estimate of the multivariable inverse actuator characteristic, R is a modal to actuator space transformation, P is a modal to Cartesian space transformation, k_p is a proportional gain, and $\hat{V}(s)$ is an estimated servo-valve dynamics model.

Three-variable controller

It is well known that variable feedback, including displacement, velocity, and acceleration feedback, can improve

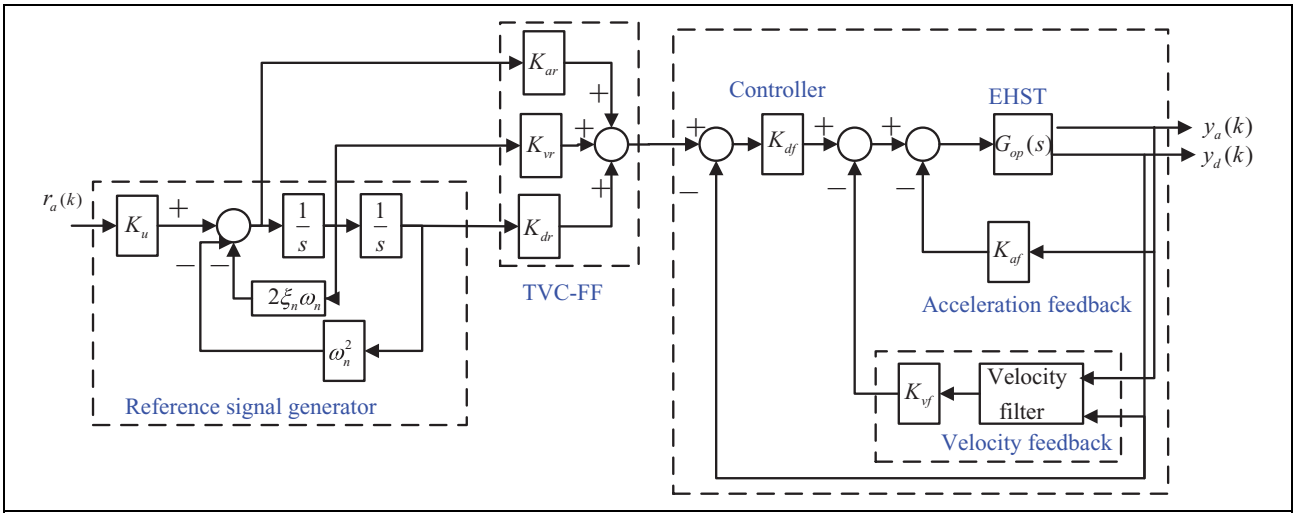

Figure 4. Block diagram of the TVC. TVC: three-variable controller.

dynamics of the EHST due to hydraulic position servo systems that regularly exhibit a poor damping ratio and a low natural frequency. Controllers based on variable feedback compensation are widely termed as a TVC.[2,18–20,30–36] A block diagram of the TVC is shown in Figure 4,[35] where K_{vf}, K_{df}, and K_{af} are three feedback parameters, and K_{dr}, K_{vr}, and K_{ar} are three feed-forward parameters, respectively. Displacement is measured by an LVDT and acceleration is measured by an accelerometer mounted on the table, and velocity is synthesized from the measured displacement and acceleration.[31] The TVC consists of a three-variable feed-forward controller (TVC-FF) and a three-variable feedback controller (TVC-FB). The TVC-FF is employed to expand the frequency bandwidth of the acceleration closed-loop system by tuning three feed-forward gain parameters $K_{ar}, K_{vr},$ and K_{dr}, and the TVC-FB is used to improve stability of the EHST by increasing the damping ratio using three feedback gain parameters $K_{af}, K_{vf},$ and K_{df}. The largest E-defense shaking table in Japan was constructed to experiment with life-size building and infrastructural system in real earthquake conditions by employing the TVC as a basic controller.[31] Wang[70] employed an acceleration feedback controller to improve stability of pneumatic actuator systems. In order to reduce the number of tuned parameters of the TVC-FF and obtain a better tracking accuracy, a feed-forward inverse model of a position closed-loop system was designed instead of the TVC-FF.[35] A dynamic pressure feedback method was employed to increase the damping ratio of the EHST in modal space controller and a better dynamic performance may be expected in the literature.[67]

Feed-forward inverse model controller

In order to obtain a reasonable acceleration waveform replication accuracy on the EHST, acceleration output responses on the EHST must match desired acceleration command signals. The EHST dynamic system consists of a proportional–integral–derivative (PID) controller, the TVC, servo-valves, hydraulic actuators, shaking table, specimen, and possibly uncertainties. Hence, how to accurately estimate position and acceleration closed-loop transfer functions of the EHST and design their inverse transfer functions is a critical issue. There are also several common identification algorithms to estimate transfer function models of the EHST such as H1,[40] a recursive least-squares (RLS) algorithm,[71–73] recursive extended least-squares (RELS) algorithm,[18,19,21,35–37,74,75] adaptive inverse identification algorithm based on least-mean-square (LMS) algorithm,[22,76] a state-space model,[40–43] genetic algorithm,[77] adaptive robust control.[78] Ozcelik et al.[79] employed an identification method based on the measured hysteresis response for a NEES-UCSD shake table mechanical system. Vasilis et al.[47] presented a discrete cosine transform LMS algorithm to estimate the acceleration closed-loop transfer function for shaking tables.

The feed-forward inverse model of position and acceleration closed-loops can be obtained by inverting the identified transfer function model or derived forward model and directly identifying the inverse model using experimental input–output data set.[80] However, the estimated discrete-time transfer function model of the EHST is a nonminimum phase (NMP) system and its direct inverse model is unstable and cannot be employed as an FIMC. In order to overcome the problem, an adaptive finite impulse response was employed to design the FIMC in practical applications,[22,76] a zero-order Taylor series approximate inverse technique was employed to synthesize a feed-forward inverse model,[81,82] and a stable approximate inverse model is designed for NMP systems in the literature.[83] Chen[46] selected three different compensation methods including an improved inverse compensation method in order to

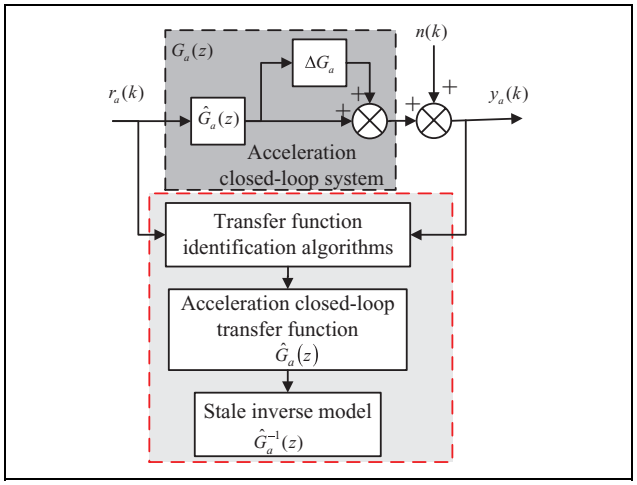

Figure 5. Block diagram of an acceleration closed-loop transfer function identification and its inversion design methods.

minimize the effect of actuator delay for real-time testing. An acceleration closed-loop model and its inverse model design method is shown in Figure 5, where $G_a(z)$ is an actual acceleration closed-loop including the coordinate controller shown in Figure 3 and the TVC shown in Figure 4, $\hat{G}_a(z)$ is an identified discrete transfer function of the acceleration closed-loop, ΔG_a describes the difference of the estimated system model $\hat{G}_a(z)$ from the actual plant $G_a(z)$, caused by noise, un-modeled dynamics, and nonlinearities,[41] the relationship $G_a(z) = \hat{G}_a(z)(1 + \Delta G_a)$, and $\hat{G}_a^{-1}(z)$ is the inverse model of the $\hat{G}_a(z)$. A stable FIMC of the identified transfer function was given by

$$\hat{G}_a^{-1}(z) = \frac{\hat{B}_u(z^{-1})\hat{A}(z)}{\hat{B}_a(z)B_u^2(1)z^{\gamma}} \tag{4}$$

where $\hat{A}(z)$ is a denominator polynomial that contains all the acceleration closed-loop system poles, which is defined by $\hat{A}(z) = z^n + a_1 z^{(n-1)} + \ldots + a_n$, $\hat{B}(z)$ is a numerator polynomial and can be decomposed into $\hat{B}_a(z)$ and $\hat{B}_u(z)$, in which $\hat{B}_a(z)$ contains all plant minimum phase zeros and $\hat{B}_u(z)$ contains all NMP zeros, which are defined by $\hat{B}_a(z) = b_{ap}z^p + b_{a(p-1)}z^{(p-1)} + \ldots + b_{a0}$ and $\hat{B}_u(z) = b_{uq}z^p + b_{u(q-1)}z^{(q-1)} + \ldots + b_{u0}$, respectively. Parameters in $\hat{A}(z)$ and $\hat{B}(z)$ can be identified by the RELS algorithm and z^{γ} is the time delay for physical realizability of $\hat{G}_a^{-1}(z)$.

In order to obtain accurate acceleration tracking performances, an FIMC of the EHST was employed to cancel out dynamic characteristics of shaking tables in the literatures[9,18–20,22,34,35,37,39,44] because the FIMC can expand the frequency bandwidth of the acceleration closed-loop system without changing its stability.[84] Lee et al.[38] employed an acceleration inverse transfer function of a shaking table to cancel out its dynamic characteristics. Della and Gründling[85] designed a cascade of compensator based on an inverse model controller to attenuate a shaker structural resonance and obtain an asymptotic reference tracking.[85] Shen et al.[21] proposed an equivalent principle between a TVC-FF and a position closed-loop inverse model to reduce tuned parameters of the EHST. Gizatullin and Edge[53] designed an FIMC to expand the frequency bandwidth of the acceleration closed-loop system for a multiaxis hydraulic test rig. Shen, Zhao and Tang designed the FIMC of acceleration,[18,19,21,86] position,[35,37] and force[74,75,87] closed-loop systems using a zero magnitude/phase error tracking technology for the EHST and an electrohydraulic control loading system, respectively. A block diagram of the FIMC for the EHST is shown in Figure 6(a), and the acceleration tracking error with the FIMC is given by

$$e_a(k) = (1+\Delta G_a)\, r_a(k) + n(k) - r_a(k) = r_a(k)\Delta G_a + n(k) \tag{5}$$

As can be seen from the aforementioned equation, the acceleration waveform replication accuracy is improved due to the FIMC. Although the FIMC can yield a better acceleration waveform replication accuracy, the EHST acceleration output responses may not perfectly replicate a desired acceleration command signal due to system uncertainties and an estimated modeling error ΔG_a in the EHST. In order to cancel out the system uncertainties and minimize the effect of the modeling error, various compensation approaches have been proposed. Vaes et al.[42,43] presented a robust multi-input multi-output (MIMO) controller based on μ-synthesis to cope with uncertainties of a designed nominal model and system nonlinearities of an electrohydraulic tractor vibration test rig. Uncertainties of an electrodynamic shaker was explicitly taken into account and an adaptive filter based on the H_∞ filtering was employed in the literature.[44] Shen et al.[18,19] employed two modeling error compensators to improve acceleration tracking dynamic characteristics of the EHST shown in Figure 6(b) and (c), respectively. A modified internal model controller[36,88,89] shown in Figure 6(d) and a real-time feedback controller with gain K_b[36,41,44] were introduced to cancel out system uncertainties and minimize the effect of a modeling error. Acceleration tracking errors with two modeling error compensators shown in Figure 6(b) and (c) and the internal model control (IMC) shown in Figure 6(d) are given by

$$e_a(k) = (1-\beta_1)\Delta G_a r_a(k) - \beta_1 r_a(k)(\Delta G_a)^2 + n(k) \tag{6}$$

$$e_a(k) = \beta_2 \Delta G_a \hat{G}_a^{-1}(z) r_a(k) + \beta(\hat{G}_a^{-1}(z)\Delta G_a)^2 r_a(k) - \hat{G}_a^{-1}(z)\Delta G_a r_a(k) \tag{7}$$

$$e_a(k) = \frac{(1+\Delta G_a)}{1+\alpha\Delta G_a} r_a(k) + \frac{1-\alpha}{1+\alpha\Delta G_a} n(k) - r_a(k) = \frac{1-\alpha}{1+\alpha\Delta G_a}(r_a(k)\Delta G_a + n(k)) \tag{8}$$

respectively. As can be seen from the aforementioned equations, the acceleration waveform replication error is

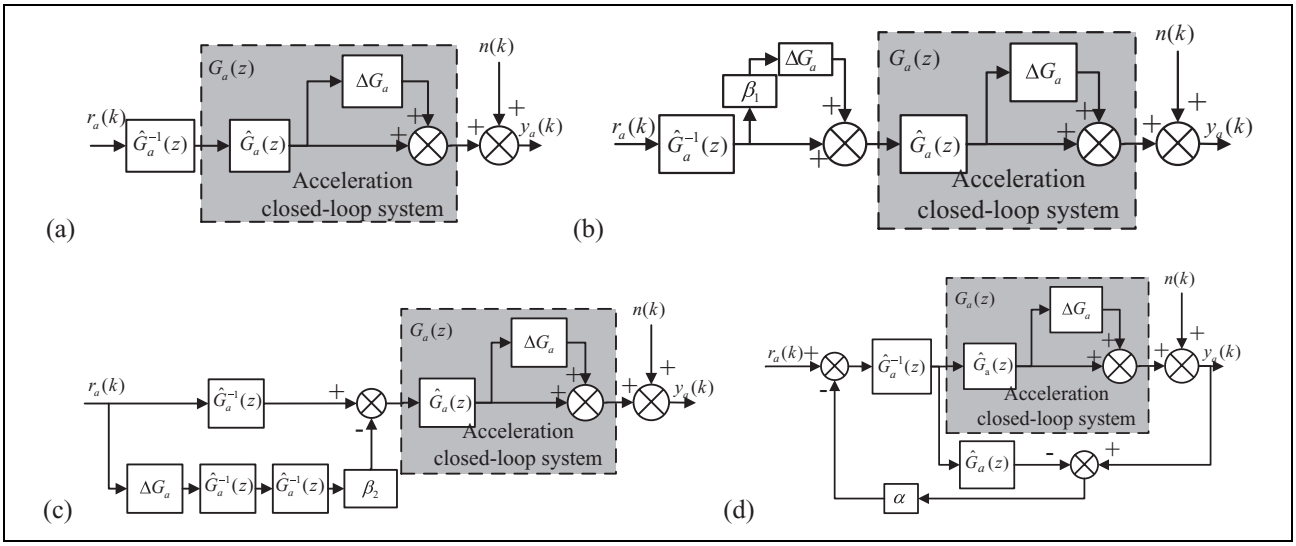

Figure 6. Feed-forward inverse model controller and its improved controllers: (a) the FIMC, (b) and (c) combined the FIMC and different MECs, and (d) combined the FIMC and the IMC. FIMC: feed-forward inverse model controller; IMC: internal model control; MEC: modeling error compensator.

decreased due to the improved internal model controller and modeling error compensators.

Off-line iterative controller

OIC has become an essential method in structural testing, automotive, and seismic testing applications.[2,20,34,36,40–44,67,90–93] The OIC based on the inverse model of a measured frequency response function of the EHST was a current industry practice approach to improve the acceleration waveform replication accuracy.[41] Various commercial packages, including MTS's remote parameter control,[67,90] iterative transfer function compensation,[2,91] Spectral Dynamics' JAGUAR MIMO waveform replication,[94] and so on, have been employed to compensate the EHST dynamic characteristics. Some main characteristics of the OIC were summarized in the literatures.[2,92] A schematic diagram of the OIC and its improved scheme in the literature[41] are shown in Figure 7(a) and (b). Experimental results showed that the improved iterative control scheme resulted in a reduction of the acceleration tracking error compared with the conventional off-line iterative control acting alone, and for the same level of tracking accuracy, the number of iterations required to the conventional off-line iterative control was reduced from 7 to 3.[41] In order to improve the control performance of an electrodynamic shaker, a real-time feedback controller with its gain K_b was added to the feedback controller.[44] Figure 7(c) shows a combined iterative control scheme[35] when the conventional off-line iterative control is augmented with a modified IMC and a real-time feedback controller K_b. In Figure 7(c), the improved IMC is introduced by tuning gain $\alpha(0 < \alpha < 1)$ to minimize the effect of ΔG_a. The acceleration output signal $y_a(k)$ of the EHST is disturbed by measurement noise $n(k)$. In the combined control scheme, acceleration tracking errors in the jth iteration with different iterative controllers in Figure 6(a) to (d) are given by

$$e^j(k) = [1 - \beta^j(1 + \Delta G_a)]e^{j-1}(k) \tag{9}$$

$$e^j(k) = [1 - \beta^j(1 + \Delta G_a)]Se^{j-1}(k) \tag{10}$$

$$e^j = \left[1 - \beta^j \frac{1 + \Delta G_a}{1 + \alpha\Delta G_a}\right] Se^{j-1} \tag{11}$$

respectively, where $S = (1 + \Delta G_a)/(K_b(1 + \Delta G_a) + 1 + \alpha\Delta G_a)$ denotes the sensitivity function of the closed-loop system. As can be seen from equations (9) to (11), the modeling error ΔG_a is an uncertainty factor only to influence the acceleration waveform replication accuracy. Therefore, combined iterative controllers shown in Figure 7(b) and (c) can accelerate convergence rate and reduce the acceleration steady-state error.

Online adaptive controller

Off-line FIMCs and iterative controllers present the following specific disadvantages for the EHST system:

- In order to obtain a better acceleration waveform replication accuracy on the EHST, the transfer function model and its inverse model of the acceleration closed-loop system must be accurately estimated and designed, respectively, and the EHST needs repetitive excitations. However, repetitive excitations will break the specimen before it is subjected to the desired excitation level.[44]
- The estimated inverse model is usually considered as time invariant and linear, but dynamic characteristics of the EHST may be changed during real-time testing. However, OICs are strongly influenced by

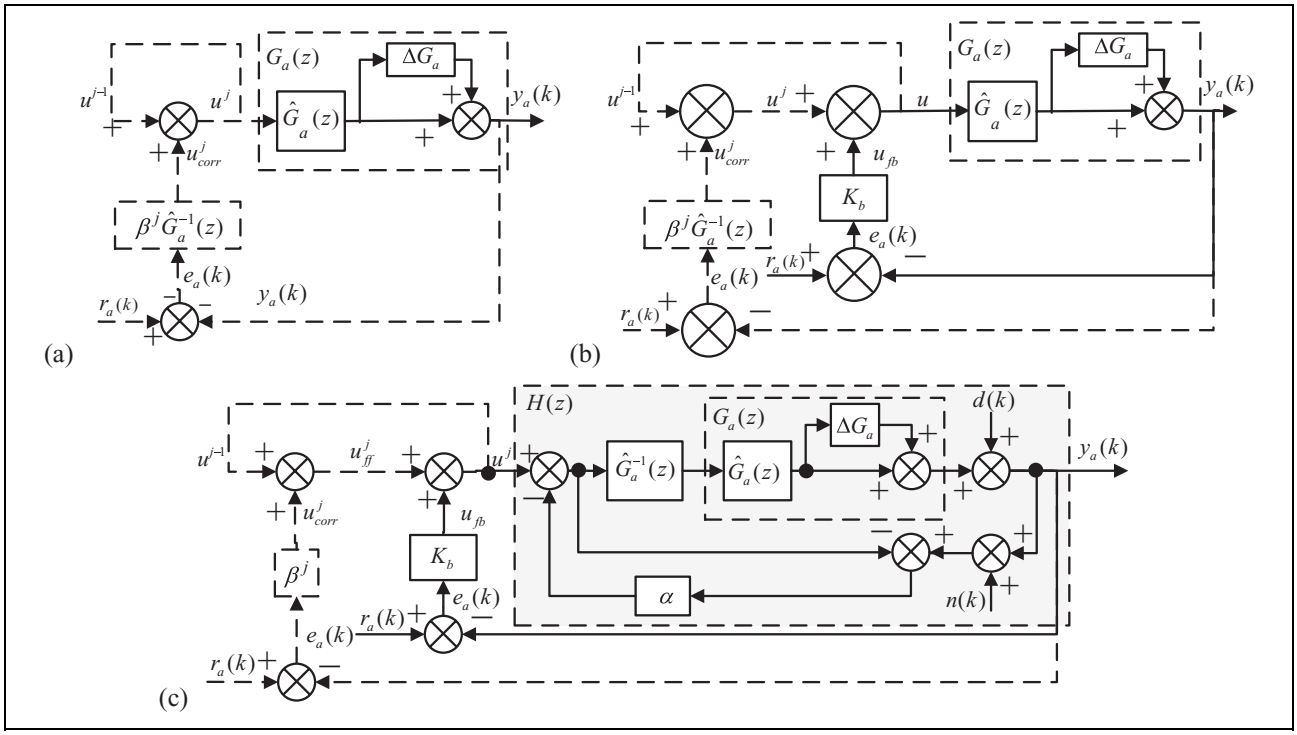

Figure 7. Off-line iterative control scheme and its improved methods: (a) a conventional iterative controller,[41] (b) combined iterative controller using an off-line feed-forward inverse model controller and a real-time feedback controller,[41] and (c) combined the conventional iterative controller and an improved IMC.[36] IMC: internal model control.

the specimen dynamics, which are nonlinear and of high order.[2]

- A real-time online iterative compensation method using inverse frequency response function may not be satisfied in the EHST system due to the computational burden of the fast Fourier transform and its inverse fast Fourier transform.
- The iterative rate of convergence and the acceleration waveform replication accuracy are closely related to the measurement and identification accuracy of the inverse model.

Hence, off-line compensation controllers, including OICs and FIMCs, and their improved methods cannot be applied in these nonlinear cases, and these shortcomings may be remedied by using an online adaptive controller in the EHST in which parameters of varying dynamics are simultaneously adapted. Some investigators turn to adaptive and intelligent control methods from off-line compensation controllers. These adaptive and intelligent control methods include AIC,[18,21,22,33,35,37,44–48] MCS,[2,18,37,40,49–53] ANFC,[27,28] APC,[20,32] AHC,[54–56] and so on.

AIC based on the LMS algorithm was first proposed by Widrow and Walach,[95] and it has been successfully employed in the EHST.[18,21,22,33,35,37,44–48] Some AIC approaches were employed for acceleration tracking control because payload dynamics are unknown and may change frequency characteristics of the EHST. Karshenas et al.[45] employed an AIC algorithm for shock testing on a shaking table. Vasilis et al.[47] presented a novel AIC framework with the LMS algorithm for accurate acceleration waveform replication in shaking tables, and the acceleration closed-loop transfer function was estimated by a discrete cosine transform LMS algorithm. Salehzadeh et al.[96] employed AIC for vibration test products, and they presented that the AIC approach was a suitable control technique in a nonlinear application such as vibration testing. An AIC scheme for the EHST system is shown in Figure 8(a), and other adaptive inverse controllers including filtered-X LMS, error-filtered, and inverse model LMS are shown in Figure 8(b) to (d), respectively, where the controller $C(z)$ is online tuned by the LMS algorithm using the reference acceleration waveform input and its tracking error $e_a(k)$ defined by $e_a(k) = d_a(k) - y_a(k) = r_a(k)M(z) - y_a(k)$, in which $M(z)$ is a reference model of the adaptive controller. The LMS algorithm for updating weights in the negative instantaneous gradient is given by

$$\boldsymbol{w}_{i+1}(k) = \boldsymbol{w}_i(k) + \lambda e_a(k)\boldsymbol{r}_a(k) \tag{12}$$

where λ is the iterative step size and $\boldsymbol{w}(k)$ is the online adaptive weight defined by $\boldsymbol{w}(k) = [w_0(k), w_1(k), \ldots, w_{m-1}(k)]^T$. The output signal of the adaptive controller to the EHST can be expressed as

$$u(k) = \boldsymbol{r}_a(k)^T C(z) = \sum_{i=0}^{m-1} r_a(k-i)w_i(k) \tag{13}$$

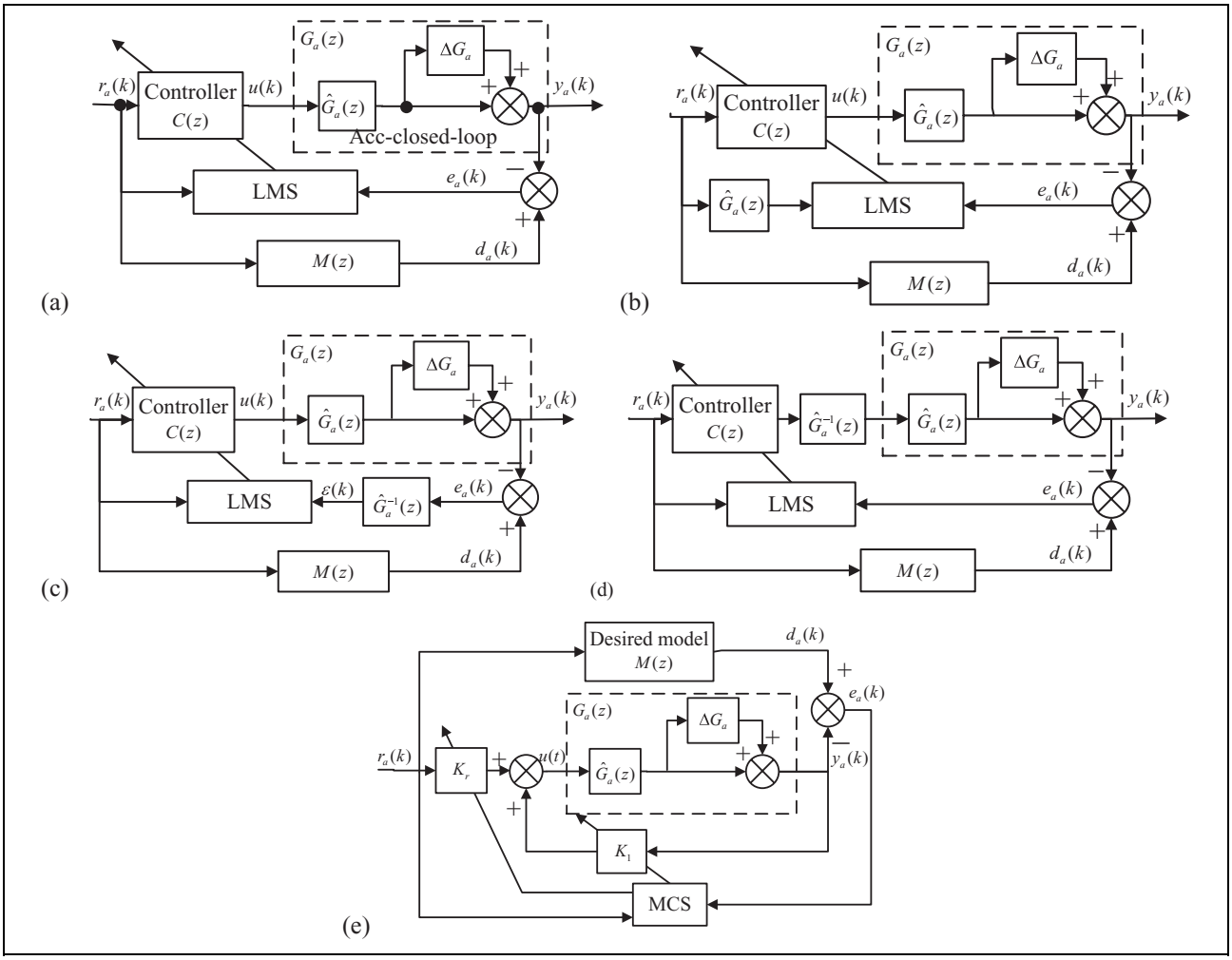

Figure 8. Adaptive controllers for the EHST: (a) LMS, (b) filtered-X LMS, (c) error-filtered LMS, (d) inverse model LMS, and (e) MCS. EHST: electrohydraulic shaking table; LMS: least-mean-square; MCS: minimal control synthesis.

The MCS algorithm was originally developed by Stoten and Benchoubane[97] as an extension to the model reference adaptive control algorithm. The MCS is widely used in electrohydraulic servo systems including the EHST.[2,18,37,40,49–53] A block diagram of the MCS structure is given in Figure 8(b). Control law of the MCS algorithm is chosen as the time-dependent state feedback strategy

$$u(t) = K_r(t)r_a(t) + K(t)y_a(t) \tag{14}$$

where the feedback gain $K \in \mathrm{R}^n$ and the feed-forward gain K_r are scalars, which are expressed as $K(t) = \int_0^t \alpha_1 e_a(\tau) y_a^T(\tau)d\tau + \beta_3 y_a^T(\tau)$ and $K_r(t) = \int_0^t \alpha_1 e_a(\tau) r_a{}^T(\tau)d\tau + \beta_3 r_a{}^T(\tau)$, in which τ is the reference vector and α_1 and β_3 are the integral weighting matrix and the proportional weighting matrix, respectively; they are usually tuned empirically and also the initial conditions are usually set to zero.[37]

Combined controller

It is well known that these adaptive control algorithms reviewed in "Online adaptive controller" section are popular approaches for the EHST system. However, these adaptive algorithms have their own advantages and disadvantages:

- High-quality waveform replication accuracy can be obtained after converging to their optimal solution.
- It is possible to exhibit poor transient response when it is initiated, especially, when the frequency bandwidth of the desired acceleration signal exceeds the frequency bandwidth of the acceleration closed-loop system of the EHST system.

Thus, there have been numerous attempts to improve the convergence rate of these adaptive control methods using some appropriate modification methods. Some combined control strategies were used to improve the tracking accuracy and the convergence rate in the EHST. Hessburg and Krantz[34] used an inverse model compensation combination with a TVC-FB to ensure stability of an EHST. August and Daniel[98] used a priori knowledge about the plant and split a controller into a long fixed part and a short adaptive part. The controller can be made more efficient by feeding back

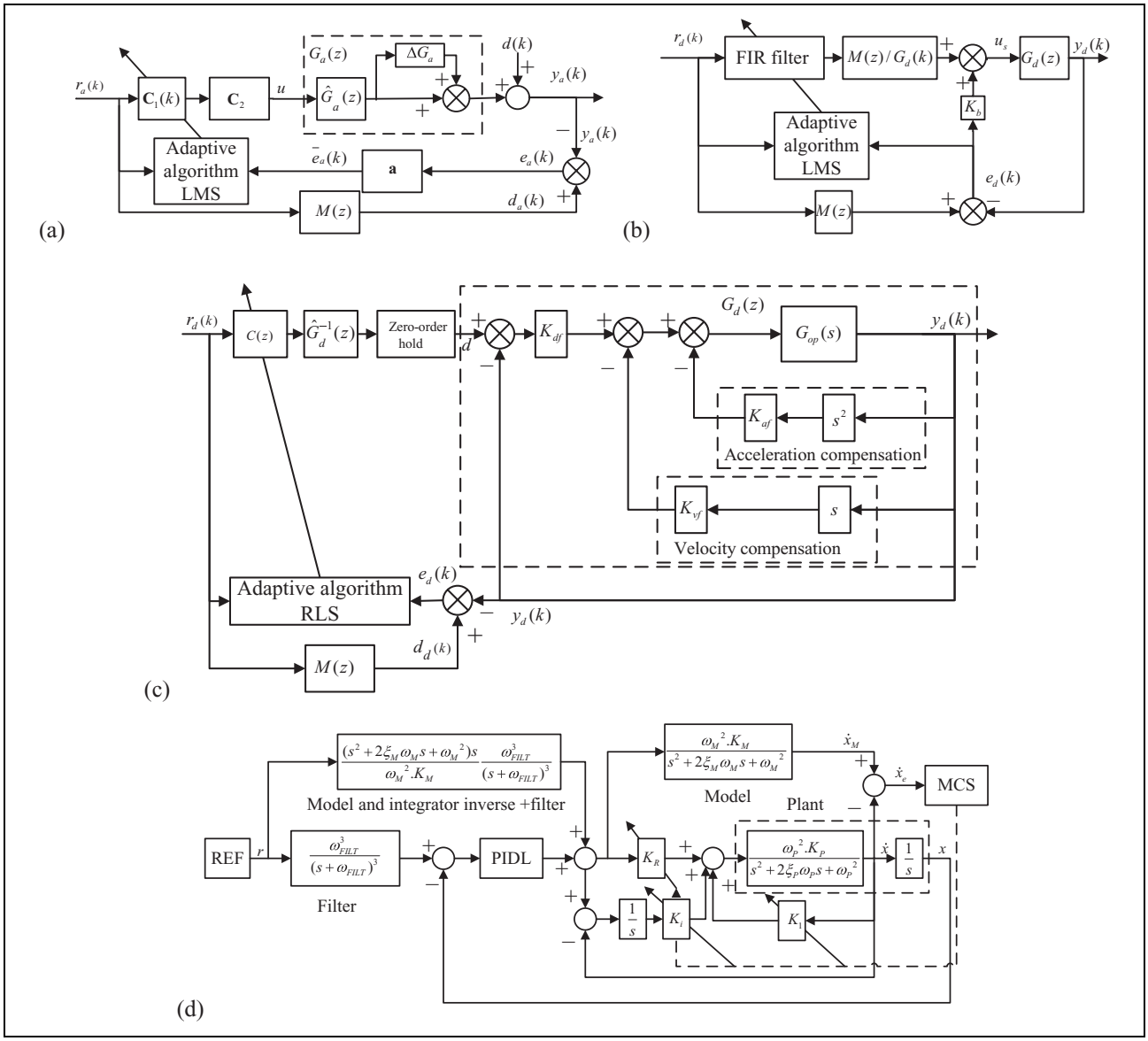

Figure 9. Combined controller for the EHST: (a) adaptive inverse controller,[98] (b) 2-DOF controller based on AIC and a real-time feedback controller,[44] (c) combined feed-forward inverse model and AIC based on the RLS,[35] (d) feed-forward inverse model and a velocity MCS,[53] (e) combined MCS with a feed-forward inverse model,[37] and (f) hybrid controller combined the FIMC and the AIC based on LMS taken modeling error into consideration.[18] EHST: electrohydraulic shaking table; DOF: degree-of-freedom; AIC: adaptive inverse control; RLS: recursive-least-squares; MCS: minimal control synthesis; FIMC: feed-forward inverse model controller; LMS: least-mean-square.

the error signal only in a desired frequency range, which is shown in Figure 9(a). Uchiyama et al.[44] developed a filtered-X LMS adaptive algorithm based on H_∞ filter and a 2-DOF controller for an electrodynamic shaker, which is shown in Figure 9(b). Shen et al.[35] proposed a combined control strategy for the EHST, which combined merits of an off-line feed-forward inverse model and an online adaptive inverse controller based on RLS algorithm because the conventional LMS has slow convergence rate and poor regulation accuracy, and the combined controller is shown in Figure 9(c). Gizatullin and Edge[53] combined an inverse model with a velocity MCS (vMCS) for a multiaxis hydraulic test rig, which is shown in Figure 9(d). The vMCS controller cascaded the overall dynamic of the EHST, and an approximate inverse model of the controlled EHST as a feed-forward compensator was used further to enhance the performance of the multiaxis hydraulic test rig. Shen et al.[37] proposed a combined controller, which combined merits of the feed-forward inverse model and the MCS to improve the position tracking accuracy of the EHST, and its integrated controller framework is shown in Figure 9(e). Shen et al.[18] proposed a hybrid controller shown in Figure 9(f), which employed an online AIC based on LMS to obtain a high accuracy of the acceleration

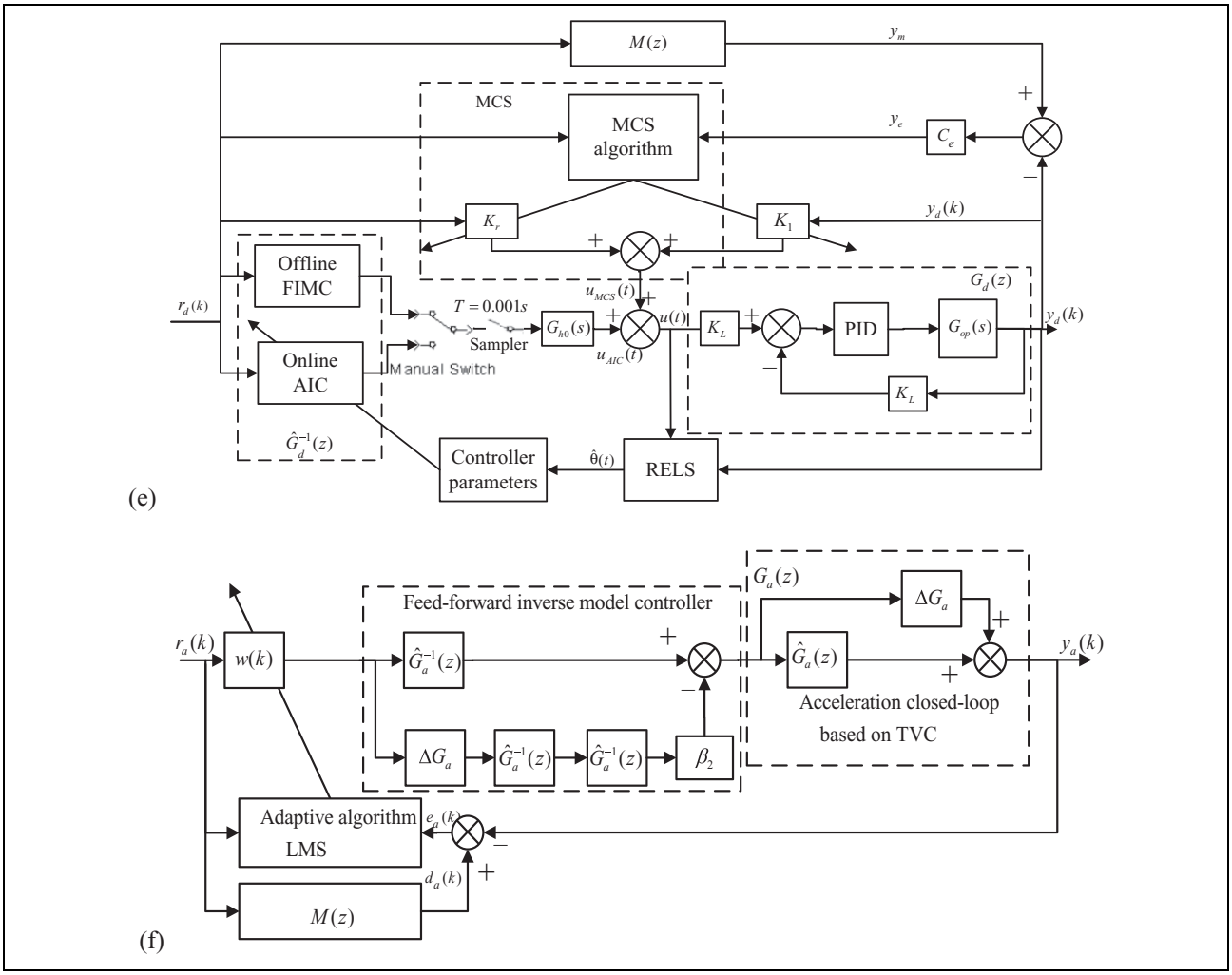

Figure 9. (Continued).

waveform after dynamic characteristics of the EHST have been improved using the TVC and the FIMC based on a modeling error compensator, which combines merits of the off-line FIMC and the online AIC.

However, the convergence performance of these combined controllers shown in Figure 9 will be directly related to the phase bandwidth of the acceleration closed-loop of the EHST.[18] If the frequency range of an acceleration command signal is larger than the phase bandwidth ($-90°$ responding to frequency) of the controlled EHST, these reviewed adaptive controllers shown in Figures 9 and 8 will search in a wrong direction and finally diverge.[99] The convergence rate and divergence condition of the LMS algorithm were given in the literatures.[100,101] An unavoidable presence of a transfer delay during acceleration transmission in shaking tables[47] and the phase delay of the acceleration closed-loop system is one of the very important factors impacting the convergence rate of the LMS algorithm[18,47] because electrohydraulic actuators and servo-valves of the EHST have an inevitable delay in response to command signals due to inherent dynamics of electrohydraulic servo systems, which bring some bad effects on the convergence rate of adaptive controllers.[38] To solve the issue, various phase delay compensators have been presented.[102–105] An adaptive controller based on a backstepping design method was proposed by Mahnaz[106] for a class of MIMO nonlinear systems with consideration of bounded time delays. An uncertain transport delay time in the transmission of an electrohydraulic servo-valve control system was presented, and a delay time variation can be effectively predicted and unconditionally removed.[107] Hence, a combined controller based on the LMS and an advanced delay compensation method[47] would produce very powerful techniques in the EHST.

Simulation evaluation analysis of main reviewed controllers

Simulation evaluation analysis for these reviewed controllers is performed in the section to verify whether these controllers can improve control performances and tracking accuracy of the acceleration waveform replication on the

Table 1. Performances comparison of main reviewed controllers.

Rank	Controllers	A	B	C	D	References
1	TVC (Figure 4)	No	–	No	No	2,18–20,30–36
2	FIMC (Figure 6(a))	No	–	No	No	9,18–20, 22, 34, 35,37, 39, 44
3	FIMC + MEC (Figure 6(b) and (c))	Yes	–	No	Yes	18,19,42, 43
4	OIC (Figure 7(a))	No	No	No	No	2,20,34,36,40–44
5	Improved OIC (Figure 7(b))	Yes	Yes	No	Yes	41
6	Combined OIC (Figure 7(c))	Yes	Yes	No	Yes	36
7	F-X LMS (Figure 8(a))	No	No	No	No	18,21,22,33,35,37,44–48
8	ε-F LMS (Figure 8(b))	Yes	Yes	Yes	No	18,95
9	MCS (Figure 8(e))	No	Yes	Yes	No	2,5,18,37,40, 49–53
10	FIMC + LMS (Figure 8(d))	Yes	Yes	Yes	No	18,35
11	FIMC + MCS (Figure 9(e))	Yes	Yes	Yes	No	37
12	FIMC + LMS + MEC (Figure 9(f))	Yes	Yes	Yes	Yes	18

TVC: three-variable controller; FIMC: feed-forward inverse model controller; MCS: minimal control synthesis; MEC: modeling error compensator; OIC: off-line iterative controller; LMS: least mean square; A: high-fidelity replication accuracy; B: convergence rate; C: real-time compensation; D: cancel out modeling error.

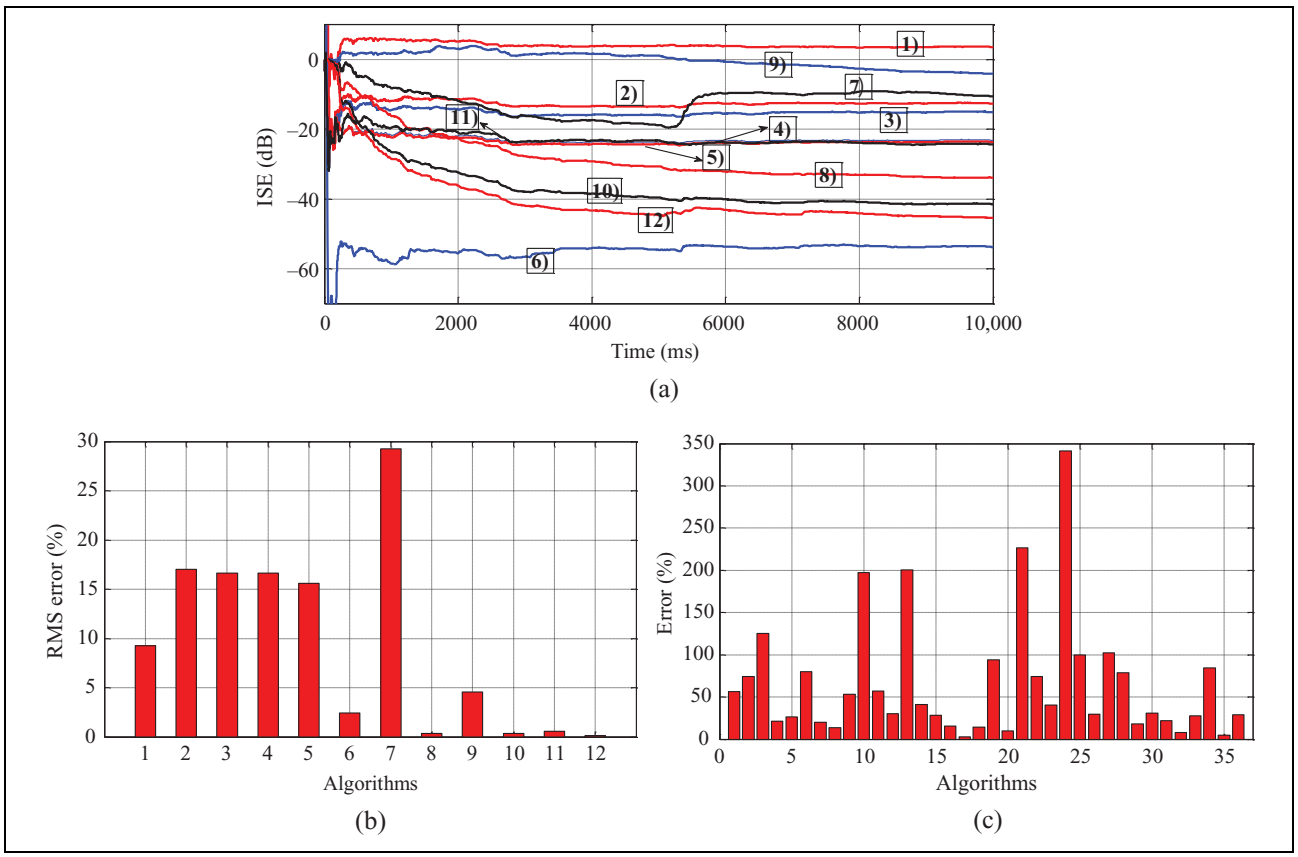

Figure 10. Comparison results of reviewed 12 controllers: (a) ISE (dB), (b) RMS (%), and (c) acceleration waveform tracking errors (%). ISE: integral of square error; RMS: root mean square.

EHST system. Advantages, drawbacks, and their references of reviewed 12 controllers are listed in Table 1. In order to evaluate performances of 12 controllers, simulation is carried out using the EHST model presented in section "Dynamic model of the EHST." A random acceleration reference signal with the frequency range of 0–20 Hz is employed to excite the nonlinear model shown in equation (1), and Figure 10(a) displays convergence results of an integral of square error (ISE, in dB). In order to quantitatively compare the acceleration tracking error of reviewed 12 controllers, a root mean square (RMS, in %) error is employed and is given by

$$\mathrm{RMS}(X_{\mathrm{in},i}, X_{\mathrm{out},i}, N) = \sqrt{\sum_{i=1}^{N} [X_{\mathrm{out},i} - X_{\mathrm{in},i}]^2} \Big/ \sqrt{\sum_{i=1}^{N} X_{\mathrm{out},i}^2} \quad (15)$$

where N is the length of reference and output signals; $X_{\text{out},i}$ and $X_{\text{in},i}$ are the reference and output signals, respectively. Figure 10(b) shows RMS comparison results of reviewed 12 controllers. A real-time acceleration waveform tracking error with three different standards including at $t = 0.1$ s, $t = 10$ s, and $\max(|r(t) - y(t)|/r(t)_{\max})$ is used to evaluate the convergence performance and tracking ability of reviewed 12 controllers. Figure 10(c) shows comparison results of real-time waveform error of reviewed 12 controllers. It can be seen that the ISE, the RMS, and the real-time waveform error are reduced, and system dynamic response has been much improved:

- The maximum ISE reduces from 5 dB with the conventional TVC controller to -55 dB with the combined OIC shown in Figure 7(c), and to -45 dB with the combined controller with the FIMC + LMS + modeling error compensator (MEC) shown in Figure 9(f).
- The maximum RMS error reduces from 9.26% with the conventional TVC controller to 2.45% with the combined OIC shown in Figure 7(c), and to 0.11% with the combined controller with the FIMC + LMS + MEC shown in Figure 9(f).
- The acceleration waveform error at $t = 10$ s reduces from 74.23% with the conventional TVC controller to 3.1% with the combined OIC shown in Figure 7(c), and to 4.5% with the combined controller with the FIMC + LMS + MEC shown in Figure 9(f).
- The acceleration time waveform error at $t = 0.1$ s reduces from 94%, 99.95%, 73.98%, 78.98%, and 84.56% to 10.08%, 29.43%, 40.38%, 18.16%, and 4.5% with different controllers, respectively.

Experimental setup of the EHST

An experimental EHST is shown in Figure 11. Specific parameters of the EHST are listed in Table 2. The EHST is controlled by six-DOF using eight servo-valves (G761-3004) manufactured by Moog Inc., Springfield, Pennsylvania, USA, with a 38 L/min flow capacity at 7 MPa supply pressure, and eight hydraulic actuators with 70 mm bore, 50 mm rod and their strokes ± 0.1 m, maximum velocity of 0.5 m/s, maximum acceleration of 2 g without payload, platform size 2×2 m^2, effective mass of 4 tons, and the acceleration frequency bandwidth of the EHST is in the range of 0–60 Hz with the TVC. Figure 12 is a schematic diagram of the EHST control system, in which eight LVDTs are attached to eight hydraulic actuators to measure their feedback displacements, and six-DOF acceleration output responses are measured by eight accelerometers mounted on the platform on the direction of each actuator. Reviewed controllers are performed in an xPC target system on the target computer. Drive signals are converted to analog signal by two D/A boards ACL-6126 and sent to eight servo-valves. Feedback signals including displacements, accelerations, and pressures are collected by two A/D boards PCI-1716.

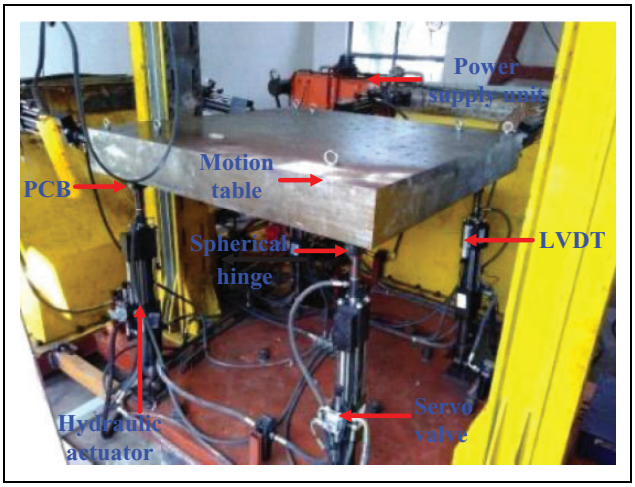

Figure 11. Experimental six-DOF EHST system. DOF: degree-of-freedom; EHST: electrohydraulic shaking table.

Table 2. Main parameters of the EHST.

Parameters	Values
Platform size	1.5×1.5 m^2
Platform weight	2000 kg
Payload	4000 kg
Maximum displacement	X: ± 100 mm; Y: ± 100 mm; Z: ± 100 mm
Maximum velocity	X: 0.5 m/s; Y: 0.5 m/s; Z: 0.5 m/s
Maximum acceleration	X: ± 2 g; Y: ± 2 g; Z: ± 2 g
Work frequency	0–60 Hz
DOF	X, Y, Z, R_x, R_y, R_z
Power supply unit	16 Mpa, 400 L/min

EHST: electrohydraulic shaking table; DOF: degree-of-freedom.

Experimental evaluation analysis of main reviewed controllers

Dynamic model verification

The open-loop dynamic model of the EHST is shown in equation (1), and magnitude and phase frequency characteristics of model and experimental results are shown in Figure 13(a) and (b), whose simulation parameters are listed in Table 3. It can be noticed from Figure 13 that the hydraulic open-loop model is able to match the actual model satisfactorily.[19]

Coordinate controller

Figure 14(a) and (b) show comparisons of differential pressure of eight hydraulic actuators with a condition of with and without the PSC, from which it can be observed that internal coupling forces of four actuators in the horizontal direction are decreased from 7MPa (supply oil pressure) to 0.3MPa and differential pressures of actuators in the vertical direction are relatively homogeneous. Experimental tuned parameters for the decoupling controller are listed in Table 4.

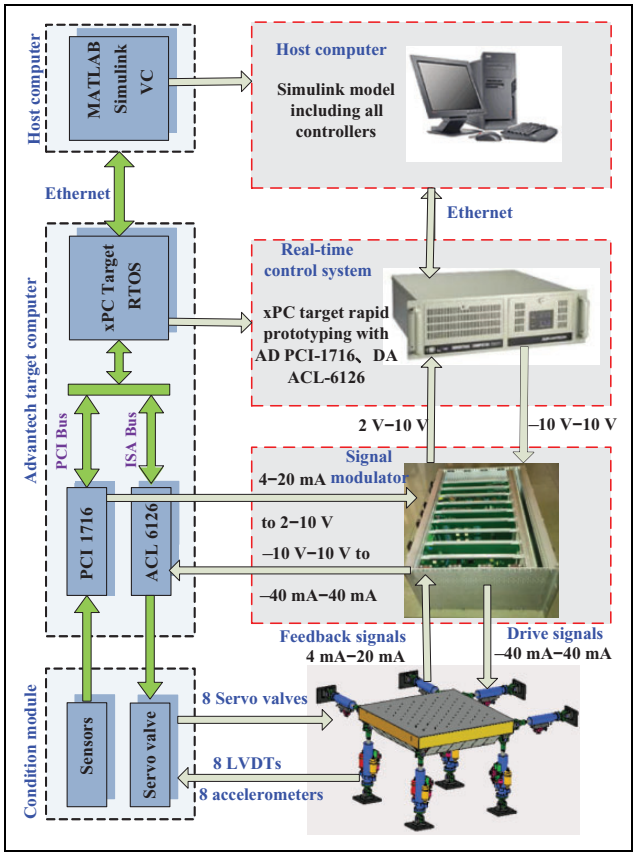

Figure 12. Schematic diagram of control system for the EHST. EHST: electrohydraulic shaking table.

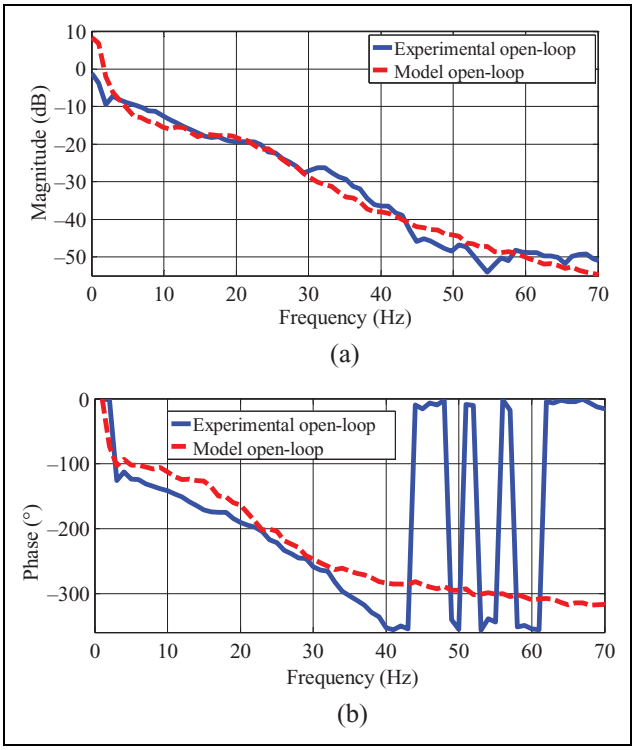

Figure 13. Comparison of open-loop model frequency characteristics between the hydraulic actuator and the actual EHST[19]: (a) magnitude and (b) phase. EHST: electrohydraulic shaking table.

Table 3. Simulation parameters of the EHST.

Parameters	Values	Parameters	Values
A_p	1.88×10^{-3} m^2	m_t	500 kg
B_p	25000 Ns/m	V_t	0.96×10^{-3} m^3
C_{ep}	4.6×10^{-17} m^3/(s/Pa)	ω_h	32Hz
C_{ip}	4.6×10^{-17} m^3/(s/Pa)	ω_{sv}	100Hz
K_q	0.00145 (m^3/s)/V	ξ_h	0.35
K_c	2×10^{-12} m^3/(s·Pa)	ξ_{sv}	0.7
K_{sv}	4 m^3/s/A	β_e	6.9×10^8 Pa

EHST: electrohydraulic shaking table.

Three-variable controller

To verify effectiveness of the TVC used in the EHST, a series of experimental tests on position and acceleration tracking control with the PID controller and the TVC have been carried out using 0.01 m position step signals, whose experimental results are shown in Figure 15. It can be seen from Figure 15 that the position tracking performance is significantly improved by using feedback gains K_{vf}, K_{df}, and K_{af} of the TVC-FB. Figure 16 presents acceleration frequency characteristics with the condition of with and without the TVC.[19] It can be seen from Figure 16 that the TVC-FF expands the frequency bandwidth of the acceleration closed loop from 25 Hz to 50 Hz in magnitude and from 12 Hz to 30 Hz in phase. Tuned main experimental parameters of the TVC are listed in Table 5.

Model identification and its inversion design

Figure 17(a) shows the comparison of frequency characteristics of the acceleration closed-loop transfer function between the actual and the estimated models in time domain, from which it can be seen that the estimated acceleration signal can match the desired acceleration command signal satisfactorily. Figure 17(b) and (c) presents the comparison of frequency characteristics of acceleration closed-loop transfer function between the actual, estimated, and designed inverse models, and Figure 17(d) and (e) presents frequency characteristics of the measured and the identified modeling errors, which indicated that the designed inverse transfer function can effectively compensate the actual acceleration closed-loop system in the interesting frequency range, and the identified modeling error can match the measured modeling error satisfactorily.[19]

Feed-forward inverse model controller

Experimental acceleration frequency characteristics using TVC, combination of TVC and FIMC, and combination of

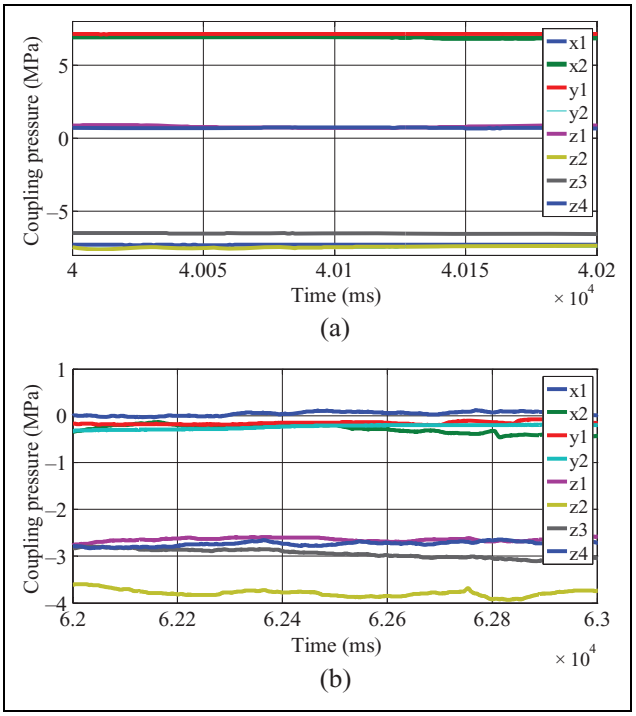

Figure 14. Coupling internal force of the redundant EHST: (a) without and (b) with the internal decoupling controller. EHST: electrohydraulic shaking table.

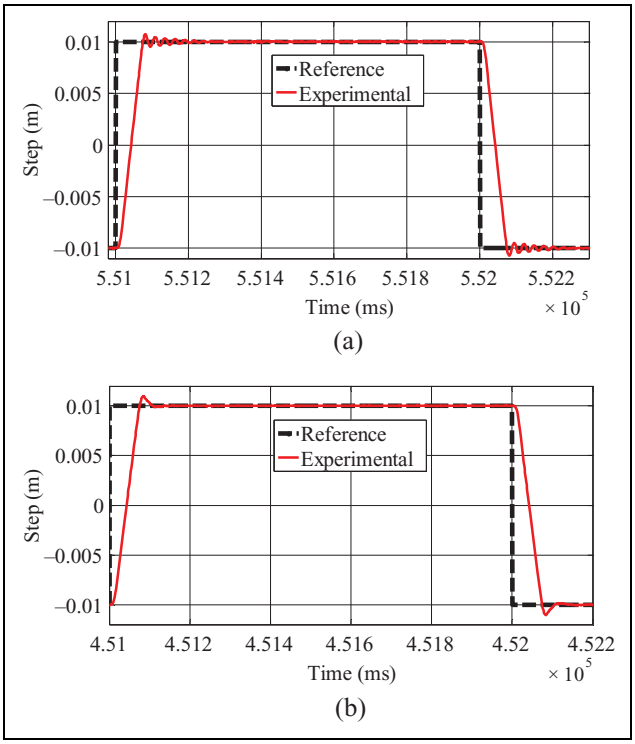

Figure 15. Experimental results excited by position step signals (a) without and (b) with the TVC-FB controllers. TVC-FB: three-variable feedback controller.

Table 4. Tuned parameters for the internal force decoupling controller.

Actuators	PSC gains	LVDT zero offset (V)	Without the PSC (MPa)	With the PSC (MPa)
x_1	−0.03	0.03	−7.35	−0.1
x_2	−0.03	−0.05	6.93	−0.17
y_1	−0.05	−0.04	7.06	0.02
y_2	−0.05	0.05	−7.58	0.06
z_1	−0.04	−0.02	0.88	−2.61
z_2	−0.03	0.09	−7.43	−3.85
z_3	−0.04	0.01	−6.56	−3.1
z_4	−0.02	−0.03	0.69	−2.66

PSC: pressure stabilizing controller; LVDT: linear variable differential transformer.

TVC, FIMC, and modeling error compensator are shown in Figure 18(a). As shown in the Figure 18(a), acceleration frequency characteristics with the TVC + FIMC perform better than that only with the TVC, and acceleration frequency characteristics can be further improved with the TVC + FIMC + MEC.[19]

Off-line iterative controller

In order to verify the effectiveness of the OIC, an acceleration random command signal with the frequency range of

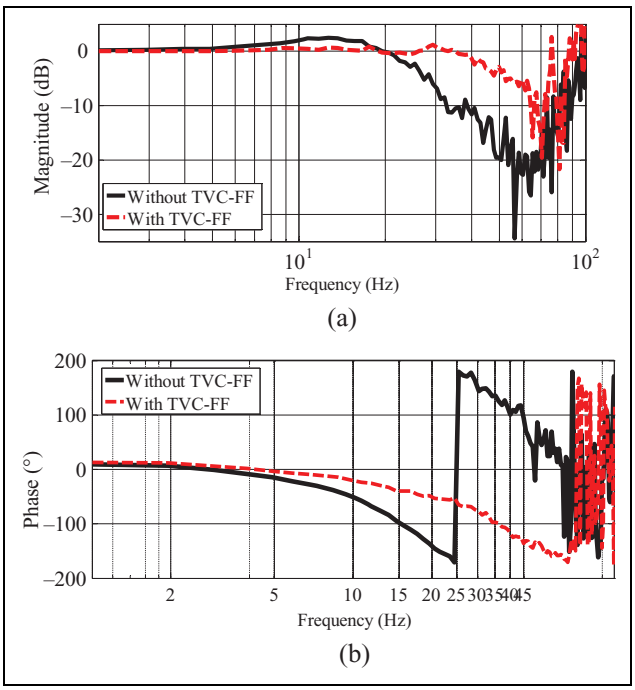

Figure 16. Acceleration frequency characteristics with and without the TVC-FFs: (a) magnitude and (b) phase. TVC-FF: three-variable feed-forward controller.

Table 5. Experimental parameters of the tuned TVC.

Parameters	Values	Parameters	Values	Parameters	Values	Parameters	Values
K_{af}	0.025	K_{ar}	0.00053	K_{df}	24.5	K_{vr}	0.84
K_{dr}	1	K_{vf}	1	ξ_n	0.7	ω_n	3.14 rad/s

TVC: three-variable controller.

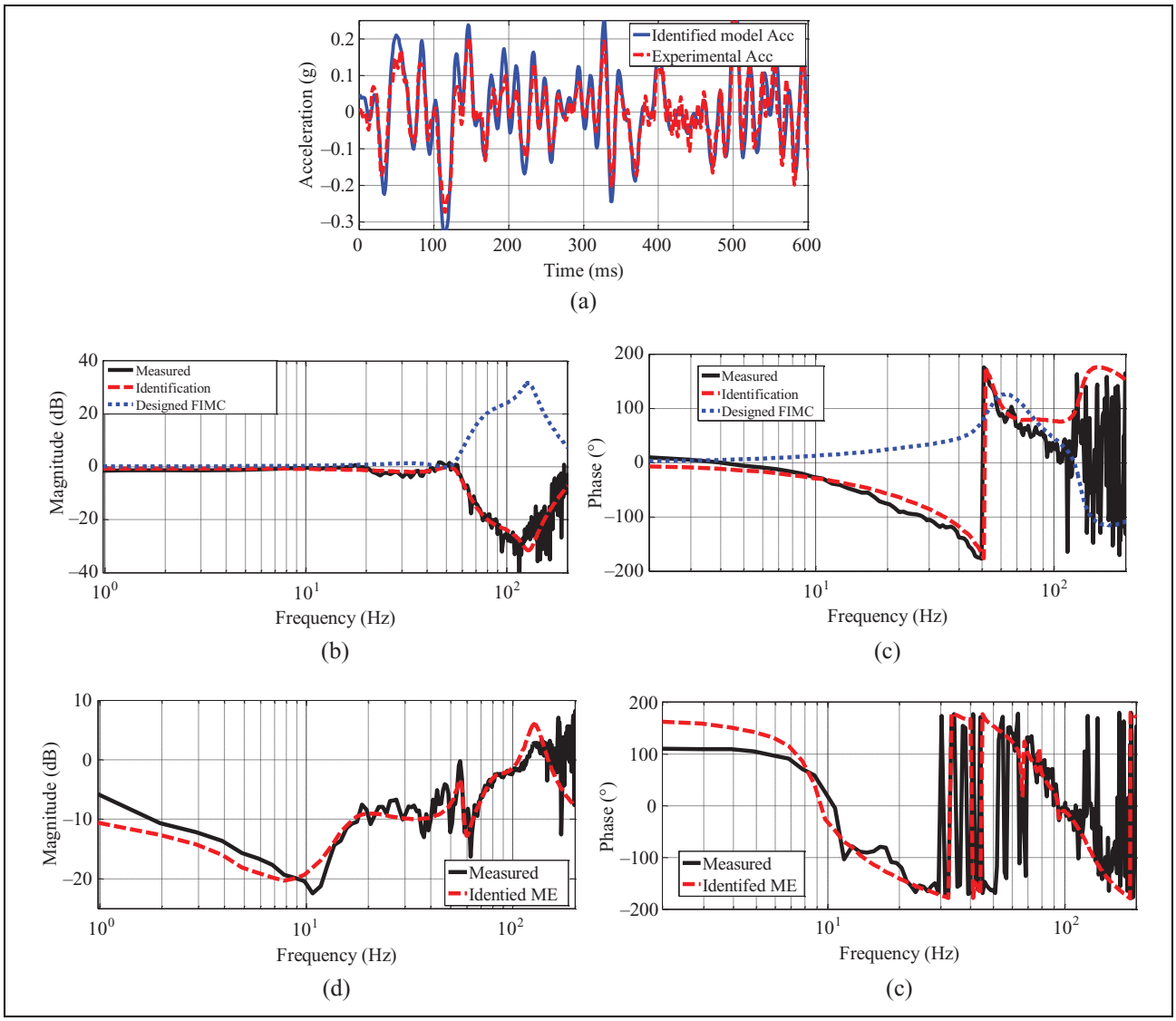

Figure 17. Comparison of the measured, identified, and designed inverse models: (a) acceleration output of the actual and identified models; acceleration closed-loop system frequency characteristics of the measured and identified models: (b) magnitude and (c) phase; acceleration modeling error frequency characteristics of the measured and identified models: (d) magnitude and (e) phase.

0–12 Hz was used to excite the nonlinear dynamic model in equation (1) and its dynamic characteristics are shown in Figure 13. Figure 19 displays an ISE iterative results. It can be seen that system dynamic response has been improved a lot, especially, the mean square error reduces from −35dB with the conventional OIC to −65dB with the improved iterative controller, as shown in Figure 7(c). To demonstrate the performance of the acceleration waveform replication using Figure 7(c), the conventional OIC is conducted without the real-time feedback controller K_b and the improved IMC is carried out as a comparison. Figure 20(a) and (b) depict the acceleration tracking error of the conventional and the improved OICs shown in Figure 7(c) after each iteration with 30 Hz sine acceleration input, and the

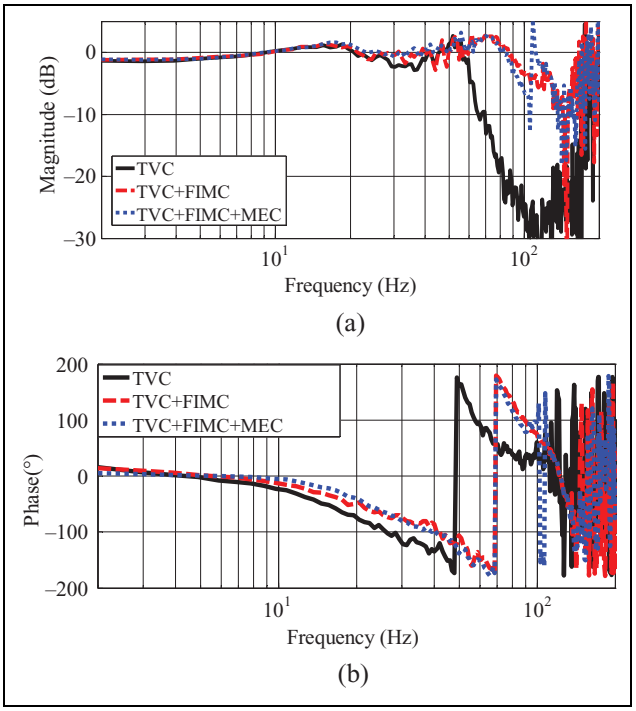

Figure 18. Experimental results of acceleration frequency characteristics with different compensators including the TVC, the TVC + FIMC, and the TVC + FIMC + MEC with $\beta_1 = 0.3$ (a) magnitude and (b) phase. TVC: three-variable controller; FIMC: feed-forward inverse model controller.

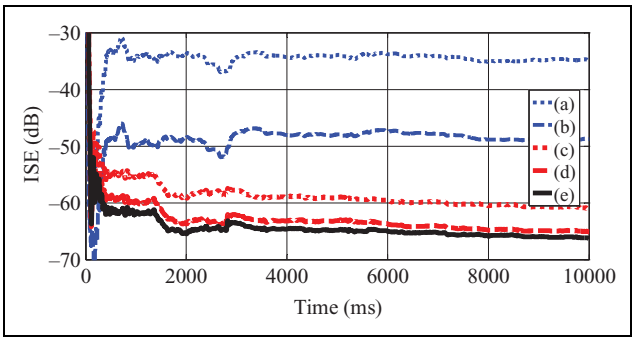

Figure 19. Simulation comparison of iteration results with different OICs: (a) the second iteration mean square error with the conventional iterative control shown in Figure 7(a) and its gain is 0.2, (b) the second iteration mean square error with the improved iterative control scheme shown in Figure 7(b) and its gain is 0.2, (c) the first iteration mean square error with the improved iterative scheme shown in Figure 7(c) and its gain is 0.3, (d) the second iteration mean square error with Figure 7(c) and its gain is 0.2, and (e) the third iteration mean square error with Figure 7(c) and its gain is 0.1. OIC: off-line iterative controller.

time domain response of two controllers after the third iteration is shown in Figure 20(c) and (d). As can be seen from Figure 7(c), the OIC exhibits a higher tracking accuracy than the conventional controller. Figure 20(e) presents the RMS error of Figure 7(a) and (c) after each iteration with sine input signal. As can be seen from Figure 20(e), the RMS error of Figure 7(a) after three iterations is 24.61%, 11.35%, and 11.05%, respectively, while that of Figure 7(c) is 15.56%, 5.32%, and 5.16%, respectively. It can be noticed that to reach the same tracking accuracy, the iterations needed are greatly reduced with Figure 7(c).

AIC and its combined controller with the FIMC

Experimental results of the acceleration waveform replication using five adaptive algorithms: (a) the LMS, (b) the filtered-X LMS, (c) the error-filtered LMS, (d) the combined controller based on the FIMC and the LMS, and (e) the hybrid controller shown in Figure 9(f) with $\beta_2 = 1$ are compared. Figure 21(a) to (e) shows comparison of the experimental results of the acceleration command signals and the measured acceleration output signals using these five adaptive algorithms with different sine signals. Figure 21(g) to (k) shows the comparison of experimental results of acceleration command signals and measured acceleration output signals using these five adaptive algorithms with the frequency range of 2–40 Hz random signal. Figure 21(f) shows comparison results of integral time-weighted absolute error (ITAE) with these five adaptive algorithms shown in Figure 21(a) to (e). Figure 21(l) shows frequency characteristics of the acceleration closed-loop system using these five adaptive algorithms shown in Figure 21(g) to (k). Consequently, experiment results in Figure 21(a) to (l) show that the hybrid controller shown in Figure 9(f) yields a more remarkable improvement in the EHST system, compared to the other controller. So, it can be concluded that the hybrid controller shown in Figure 9(f) is effective in the acceleration waveform replication and meets the experimental requirement of the EHST.

MCS and its combined controller with the FIMC

Comparisons of the position command and the measured displacement output with the traditional PID controller, the MCS, and the FIMC + MCS are shown in Figure 22(a)-(c), respectively, which are excited by the frequency range of 0-15Hz random signals. As can be seen from Figure 22, the acceleration tracking waveform performance with the FIMC + MCS can be greatly improved compared to the conditional PID controller and the MCS alone. Frequency response characteristics of the EHST position closed-loop system with the FIMC + MCS and the PID controller are compared in Figure 22(e). Comparison of experimental results show that the frequency bandwidth of the position closed-loop system in the EHST already increased up to 40 Hz according to the $-100°$ phase condition.

Combined controller with the FIMC and the adaptive RELS

Comparison of the position command and the measured position output in time domain excited by a random signal

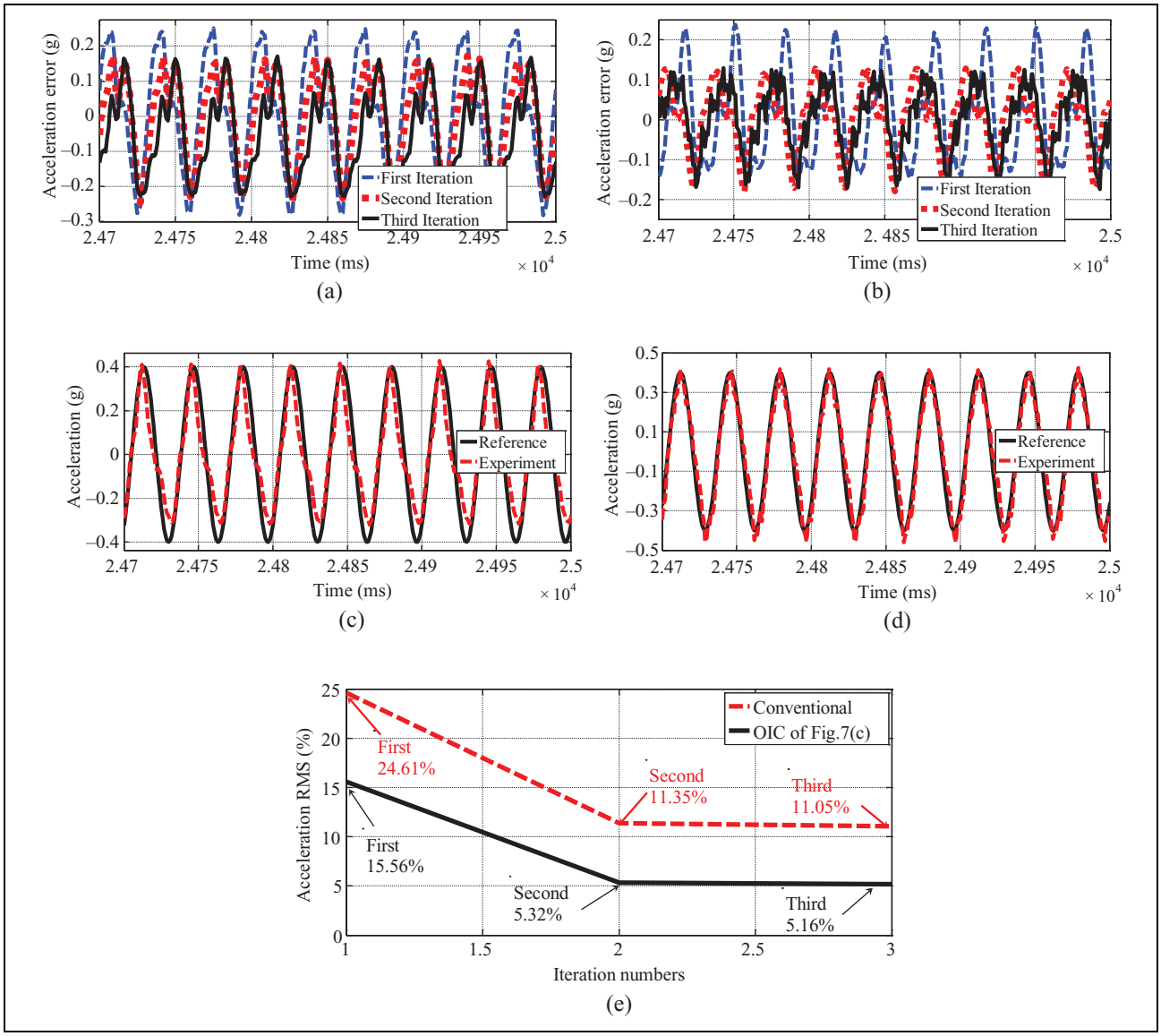

Figure 20. Experimental results of acceleration tracking error with sine input after each iteration: (a) conventional pure off-line iterative control shown in Figure 7(a) and (b) improved OIC shown in Figure 7(c); acceleration output responses with sine input after each iteration: (c) and (d) are conventional OIC shown in Figure 7(a) and improved OIC shown in Figure 7(c), and (e) acceleration RMS error after each iteration with sine input signal. OIC: off-line iterative controller; RMS: root mean square.

with the frequency range of 0–20 Hz using the traditional PID controller, PID with feedback compensation, the FIMC, and the FIMC + RLS shown in Figure 9(c) is shown in Figure 23(a), and comparison of acceleration output responses using the FIMC + RLS is shown in Figure 23(b). It can be seen from Figure 23 that the position and the acceleration tracking performances with the FIMC + RLS are more satisfactory than those with the PID controller, the PID with feedback compensation, and the FIMC.

Concluding remarks

A number of control techniques have been investigated extensively in recent years to improve the acceleration waveform replication accuracy on EHSTs. In the article, an experimental EHST and its nonlinear model are established to verify acceleration tracking control performances of these reviewed controllers. Different controllers have been addressed including the PID controller, the TVC controller and its improved controllers, the FIMC and its improved controller combined with modeling error, and adaptive controllers and their combined controllers. To compare control performances of these controllers, a number of experiments are carried out on an actual EHST system. From these simulation and experimental results of the acceleration waveform replication, the following conclusions can be made:

1. A coordinate controller is the most important controller to decouple the internal coupling force in the

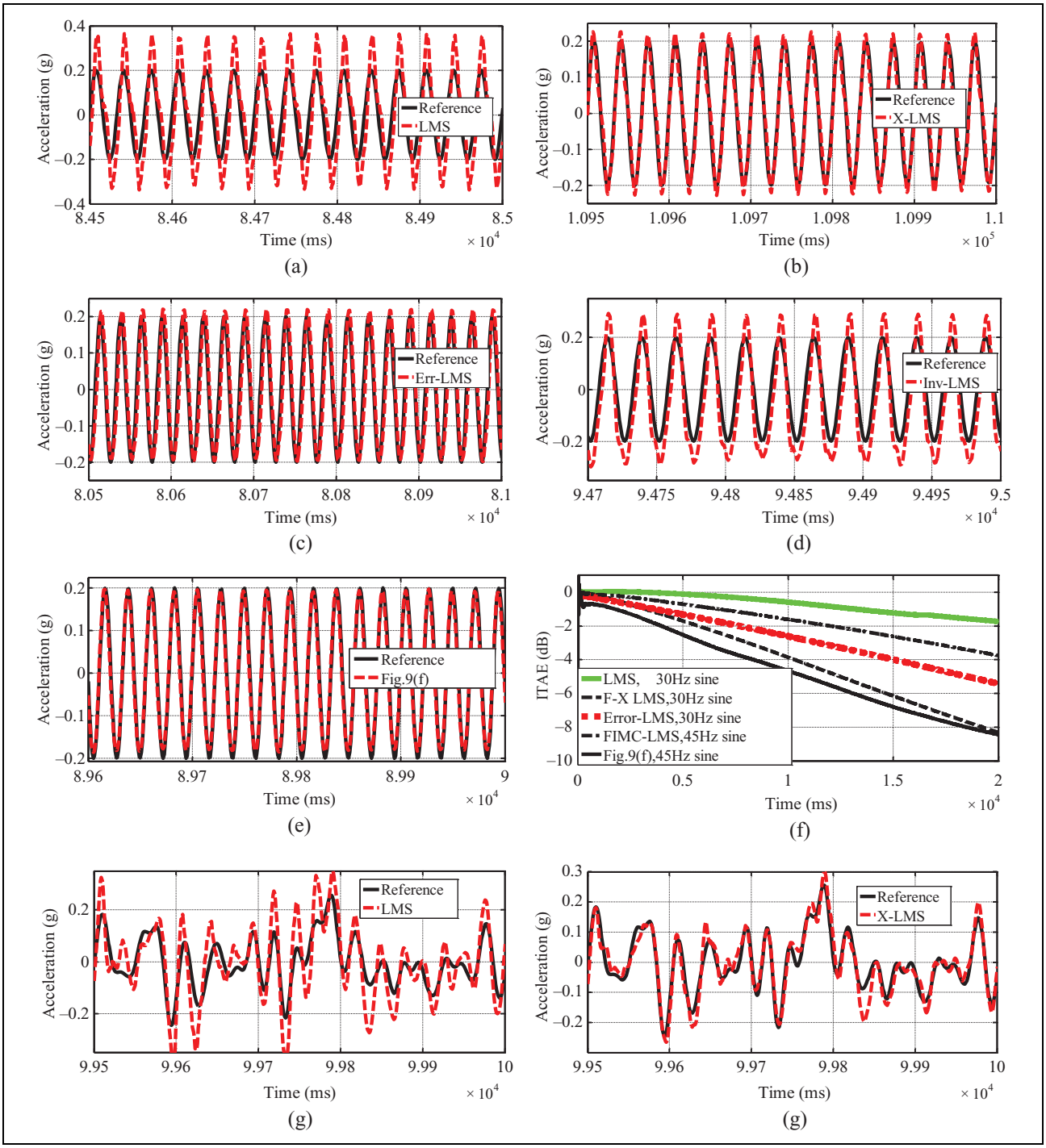

Figure 21. Experimental results of different adaptive controllers with different acceleration reference signals: (a) LMS with 30 Hz sine, (b) filtered-X LMS with 30 Hz sine, (c) error-filtered LMS with 30 Hz sine, (d) combined the FIMC and the LMS with 45 Hz sine, (e) the hybrid controller shown in Figure 9(f) with 45 Hz sine, (f) ITAE for different AICs with different reference signals, (g) LMS, (h) filtered-X LMS, (i) error-filtered LMS, (j) combined the FIMC and the LMS, (k) the hybrid controller shown in Figure 9(f) with the frequency range of 2–40 Hz random signal, and (l) frequency characteristics of Figure 21(g) to (k). LMS: least-mean-square; FIMC: feed-forward inverse model controller; AIC: adaptive inverse control; ITAE: integral time-weighted absolute error.

redundant EHST because geometric effects, different parameters, and installation error of the eight actuators can cause the EHST cannot work normally. Hence, the coordinate controller, including the transform matrix, the PSC, and the PID controller, of the redundant EHST must be designed and tuned first.

2. The most popular controller applied in the EHST is a PID controller, but it can only improve the

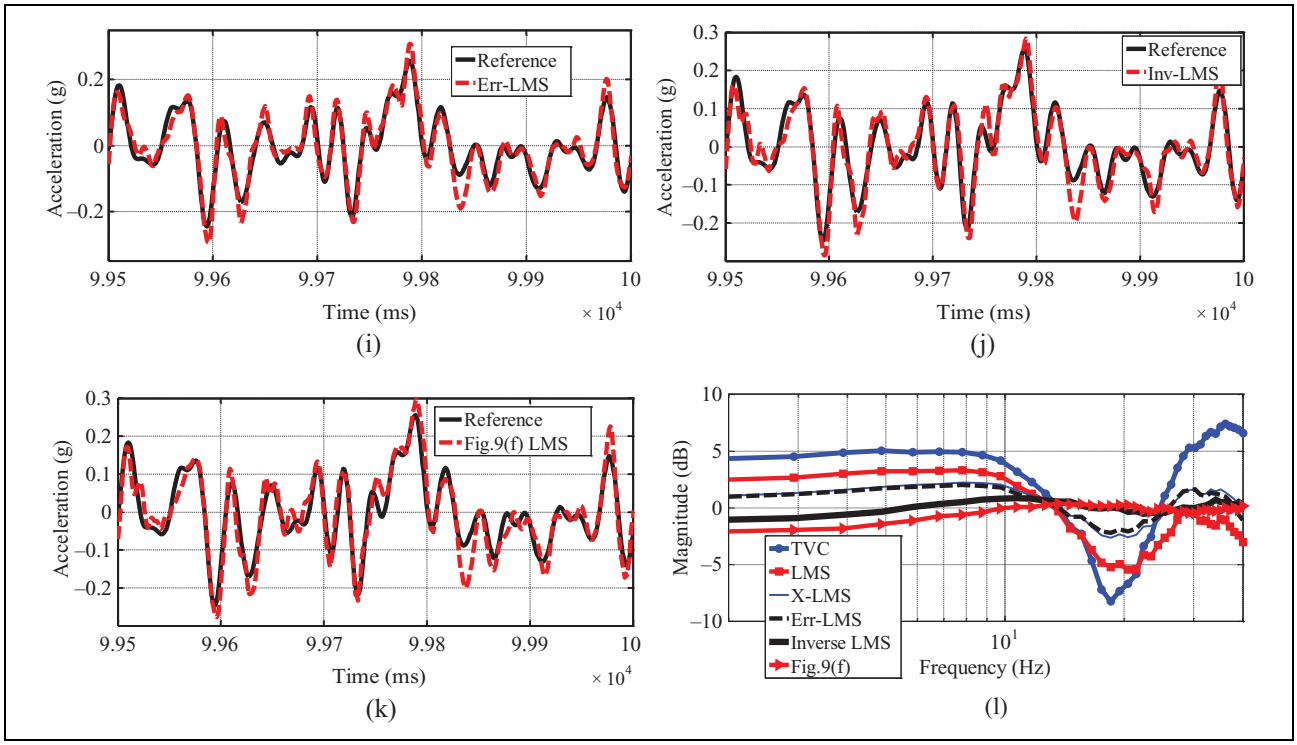

Figure 21. (Continued).

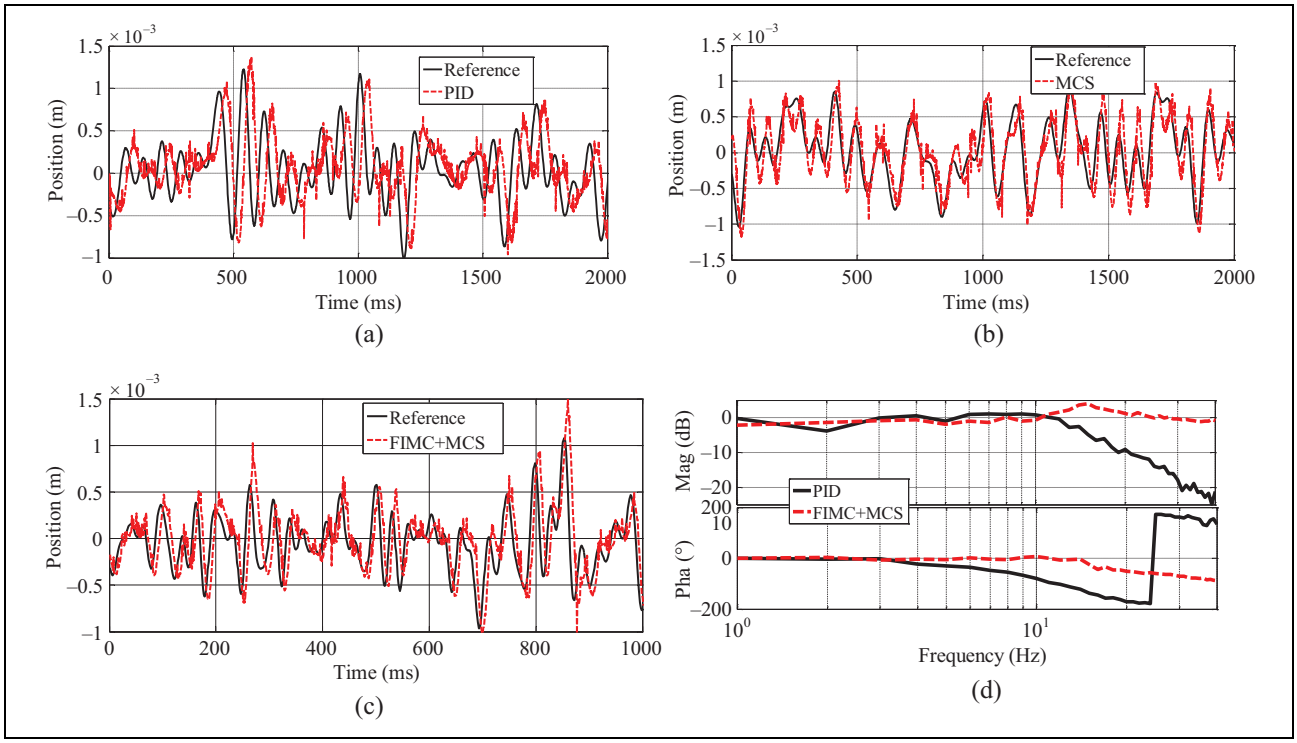

Figure 22. Experimental results of the position tracking control: (a) the PID, (b) the MCS, (c) combined controller based on the FIMC + MCS with the range of 0–15 Hz position random signal, and (d) comparison of frequency characteristics using the PID and the FIMC + MCS with the range of 0–40 Hz position random signal. PID: proportional-integral-derivative; MCS: minimal control synthesis; FIMC: feed-forward inverse model controller.

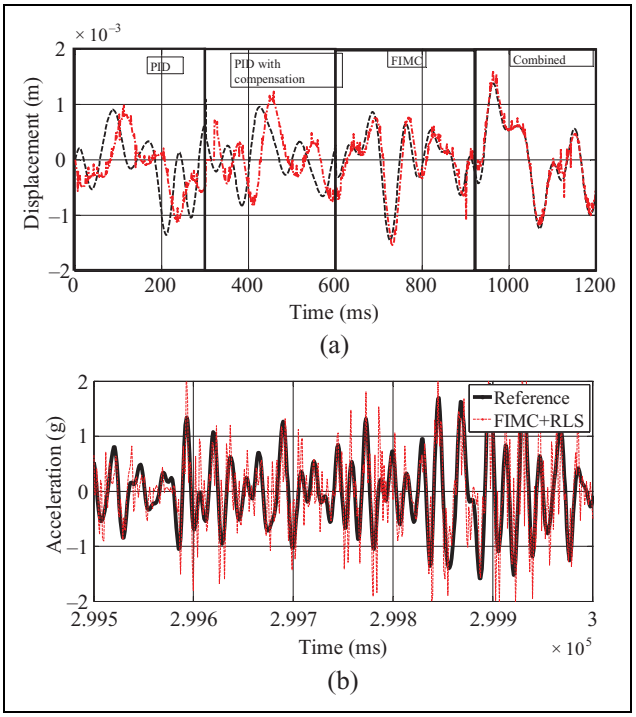

Figure 23. Experimental results of the position and the acceleration tracking control with different controllers: (a) the position tracking with the PID controller, the PID with the acceleration and the velocity feedback compensation, the FIMC, and the FIMC + RLS and (b) acceleration output responses with the FIMC + RLS. PID: proportional-integral-derivative; FIMC: feed-forward inverse model controller; RLS: recursive-least-squares.

acceleration waveform replication accuracy in a very limited range because hydraulic position servo systems regularly exhibit a poor damping ratio and a lower frequency bandwidth. A compensated PID controller using the velocity and the acceleration feedback compensation can improve the natural frequency and the damping ratio of the EHST.

3. The TVC is a commonly used controller employed in the EHST because it can expand the frequency bandwidth of the acceleration closed-loop system by tuning TVC-FF and increase the damping ratio and stability of the EHST by tuning TVC-FB. The TVC is employed in engineering applications including the largest E-Defense shaking table in Japan.
4. Feed-forward inverse model compensation methods improve the acceleration waveform replication accuracy significantly, but a modeling error occurs between the estimated model and the designed inverse model with the actual model of the EHST and system uncertainties; so, some combined controllers, including a modeling error compensator and an internal model controller, are designed to solve the problem. Some compensation methods of the stable inverse model must be studied because the identified model of the acceleration closed-loop system is a nonminimum phase system and its inverse model is unstable.
5. Off-line compensation controllers, including the TVC controller, the FIMC, and the OIC, can yield a better frequency bandwidth of the EHST using feed-forward and feedback compensation, but they cannot adaptively tune parameters to suppress variable dynamic characteristics of the EHST during real-time testing. Hence, a high-fidelity acceleration waveform cannot replicate on the EHST. Some adaptive controllers can obtain a high-quality acceleration waveform replication after convergence to their optimal solution, but they are possible to exhibit poor transient response when the frequency bandwidth of the desired acceleration signal exceeds the frequency bandwidth of the acceleration closed-loop system.
6. Some combined controllers including FIMC + AIC/MCS/RLS can accelerate the convergence rate of these adaptive controllers and improve the acceleration tracking accuracy. These combined controllers combined the advantages of online adaptive controllers, off-line FIMCs, modeling error compensators, the IMC, time delay compensators, and so on. Combination of these several research areas has given promising results in a few studies. These combined controllers can extend to other control systems.
7. The coordinate controller and the PID controller are tuned first, the TVC-FB is then employed to improve the stability of the EHST, and the TVC-FF is then employed to expand the frequency bandwidth of the acceleration closed-loop system. A complete servo controller for the EHST is implemented. The FIMC, the OIC, and their combined methods can be used to further improve acceleration frequency characteristics and expand the frequency bandwidth of the acceleration closed-loop system. Online adaptive controllers and their combined methods can be employed finally to obtain a high-fidelity acceleration waveform accuracy if fixed dynamic characteristics of the EHST are changed during real-time testing subjected to disturbances.

Consequently, these reviewed control techniques not only be utilized for the six-DOF redundant EHST but also are effective methods for the other closed-loop control systems.

Acknowledgment

The authors would like to thank the editor, associate editors and anonymous reviewers for their constructive comments.

Declaration of conflicting interests

The author(s) declared no potential conflicts of interest with respect to the research, authorship, and/or publication of this article.

Funding

The author(s) disclosed receipt of the following financial support for the research, authorship, and/or publication of this article: This research was supported by the National Natural Science Foundation of China (no. 51575511), the Fundamental Research Funds for the Central Universities in China (no. 2015XKMS025), the Priority Academic Program Development of Jiangsu Higher Education Institutions (PAPD), and the Qing Lan Project in Jiangsu province.

References

1. Severn RT. The development of shaking tables-a historical note. *Earthquake Eng Struct Dynam* 2011; 40(2): 195–213.
2. Plummer AR. Control techniques for structural testing: a review. *Proc Inst Mech Eng* 2007; 221(3): 139–169.
3. Luco JE, Ozcelik O, and Conte JP. Acceleration tracking performance of the UCSD-NEES shake table. *J Struct Eng* 2010; 136: 481–490.
4. Chen C and Ricles JM. Stability analysis of explicit integration algorithms with actuator delay for real-time hybrid testing. *Earthquake Eng Struct Dynam* 2008; 37(4): 597–613.
5. Chen C and James MR. Analysis of actuator delay compensation methods for real-time testing. *Eng Struct* 2009; 31(11): 2643–2655.
6. Kim JW, Xuan DJ, and Kim YB. Design of a forced control system for a dynamic road simulator using QFT. *Int J Automot Technol* 2008; 9(1): 37–43.
7. Kim JW, Xuan DJ, and Kim YB. Robust control application for a three-axis road simulator. *J Mech Sci Technol* 2011; 25(1): 221–231.
8. Ji XD, Kajiwara K, Nagae T, et al. A substructure shaking table test for reproduction of earthquake response of high-rise buildings. *Earthquake Eng Struct Dynam* 2009; 38: 1381–1399.
9. Lee SK, Park EC, and Min KW. Real-time hybrid shaking table testing method for the performance evaluation of a tuned liquid damper controlling seismic response of building structures. *J Sound Vib* 2007; 302: 596–612.
10. Wang T, Yoshitake N, Pan P, et al. Numerical characteristics of peer-to-peer (P2P) internet online hybrid test system and its application to seismic simulation of SRC structure. *Earthquake Eng Struct Dynam* 2008; 37: 265–282.
11. Nield SA, Stoten DP, Drury D, et al. Control issues relating to real-time sub-structuring experiments using a shaking table. *Earthquake Eng Struct Dynam* 2005; 34: 1171–1192.
12. Shi ZM, Wang YQ, Peng M, et al. Characteristics of the landslide dams induced by the 2008 Wenchuan earthquake and dynamic behavior analysis using large-scale shaking table tests. *Eng Geol* 2015; 194(26): 25–37.
13. Han JW, Kim JD, and Song SY. Fatigue strength evaluation of a bogie frame for urban maglev train with fatigue test on full-scale test rig. *Eng Fail Anal* 2013; 31: 412–420.
14. Xu ZD. Horizontal shaking table tests on structures using innovative earthquake mitigation devices. *J Sound Vib* 2009; 325(1–2): 34–48.
15. McCrum DP and Williams MS. An overview of seismic hybrid testing of engineering structures. *Eng Struct* 2016; 118: 240–261.
16. Plummer A. A general co-ordinate transformation framework for multi-axis motion control with application in the testing industry. *Contr Eng Pract* 2010; 10: 598–607.
17. Plummer AR. Model-based motion control for multi-axis servohydraulic shaking tables. *Contr Eng Pract* 2016; 53: 109–122.
18. Shen G, Zhu ZC, Zhang L, et al. Adaptive feed-forward compensation for hybrid control with acceleration time waveform replication on electro-hydraulic shaking table. *Contr Eng Pract* 2013; 8(21): 1128–1142.
19. Shen G, Zhu ZC, Li X, et al. Real-time electro-hydraulic hybrid system for structural testing subjected to vibration and force loading. *Mechatronics* 2016; 33: 49–70.
20. Yao JJ, Matt DM, Xiao R, et al. An overview of control schemes for hydraulic shaking tables. *J Vib Contr* 2016; 22(12): 2807–2823.
21. Shen G, Zheng ST, Ye ZM, et al. Adaptive inverse control of time waveform replication for electrohydraulic shaking table. *J Vib Contr* 2011; 17(11): 1611–1633.
22. Shen G, Zhu ZC, Tang Y, et al. Combined control strategy using internal model control and adaptive inverse control for electro-hydraulic shaking table. *Proc Inst Mech Eng* 2013; 227(10): 2348–2360.
23. Yao JY, Jiao ZX, and Ma DW. Extended-state-observer-based output feedback nonlinear robust control of hydraulic systems with backstepping. *IEEE Trans Ind Electron* 2014; 61: 6285–6293.
24. Yao JY, Jiao ZX, Ma DW, et al. High-accuracy tracking control of hydraulic rotary actuators with modeling uncertainties. *IEEE/ASME Trans Mechatron* 2014; 19: 633–641.
25. Guo K, Wei JH, and Fang JH. Position tracking control of electro-hydraulic single-rod actuator based on an extended disturbance observer. *Mechatronics* 2015; 207: 47–56.
26. Plummer AR. A detailed dynamic model of a six-axis shaking table. *J Earthquake Eng* 2008; 12(4): 631–662.
27. Kenta S and Makoto I. Adaptive compensation for reaction force with frequency variation in shaking table systems. *IEEE Trans Ind Electron* 2009; 56(10): 3864–3871.
28. Kenta S, Makoto I, and Yasuda K. Adaptive feedforward compensation for reaction force with nonlinear specimen in shaking tables. In: *Proceeding of the 2009 IEEE International Conference on Mechatronic*, Malaga, Spain 1–6, 2009
29. Stehman M and Nakata N. Direct acceleration feedback control of shake tables with force stabilization. *J Earthquake Eng* 2013; 17: 736–749.
30. Xu Y, Hua HX, and Han JW. Modeling and controller design of a shaking table in an active structural control system. *Mech Syst Signal Process* 2008; 2: 1917–1923.
31. Tagawa Y and Kajiwara K. Controller development for the E-Defense shaking table. *Proc Inst Mech Eng* 2007; 221(2): 171–181.
32. Yao JJ, Di DT, Jiang GL, et al. Acceleration amplitude-phase regulation for electro-hydraulic servo shaking table based on

LMS adaptive filtering algorithm. *Int J Contr* 2012; 85(10): 1581–1592.
33. Yao JJ, Wang XC, Hu SH, et al. Adaline neural network-based adaptive inverse control for an electro-hydraulic servo system. *J Vib Control* 2011; 17(13): 2007–2014.
34. Hessburg TM and Krantz DG. Feedforward control (based on model inversion) and system performance prediction using high-fidelity nonlinear dynamic hydraulic system modeling. In: *Proceedings of the 1997 IEEE International Conference on Control Applications*, Hartford, Connecticut, USA, 5–7 October 1997, pp. 57–62.
35. Shen G, Zheng ST, Ye ZM, et al. Tracking control of an electro-hydraulic shaking table system using a combined feedforward inverse model and adaptive inverse control for real-time testing. *Proc Inst Mech Eng* 2011; 225: 647–666.
36. Tang Y, Shen G, Zhu ZC, et al. Time waveform replication for electro-hydraulic shaking table incorporating off-line iterative learning control and modified internal model control. *Proc Inst Mech Eng* 2014; 228(9): 722–733.
37. Shen G, Lv GM, Cong DC, et al. Implementation of electro-hydraulic shaking table controllers with a combined adaptive inverse control and minimal control synthesis algorithm. *IET Contr Theor Appl* 2011; 5(13): 1471–1483.
38. Lee SK, Park EC, Min KW, et al. Real-time substructuring technique for the shaking table test of upper substructures. *Eng Struct* 2007; 29(9): 2219–2232.
39. Chen C and James MR. Improving the inverse compensation method for real-time hydrid simulation through a dual compensation scheme. *Earthquake Eng Struct Dynam* 2009; 38: 1237–1255.
40. Cuyper JD and Verhaegen M. State space modeling and stable dynamic inversion for trajectory tracking on an industrial sat test rig. *J Vib Contr* 2002; 8: 1033–1050.
41. Cuyper JD, Verhaegen M, and Swevers J. Off-line feedforward and $H\infty$ feedback control on a vibration rig. *Contr Eng Pract* 2003; 11: 129–140.
42. Vaes D, Engelen K, Anthonis J, et al. Multivariable feedback design to improve tracking performance on tractor vibration test rig. *Mech Syst Signal Process* 2007; 21: 1051–1075.
43. Vaes D, Swevers J, and Sas P. Experimental validation of different MIMO-feedback controller design methods. *Contr Eng Pract* 2005; 13: 1439–1451.
44. Uchiyama Y, Mukai M, and Fujita M. Robust control of electrodynamic shaker with 2dof control using $H\infty$ filter. *J Sound Vib* 2009; 326: 75–87.
45. Karshenas AM, Dunnigan MW, and Williams BW. Adaptive inverse control algorithm for shock testing. *IEE Proc Contr Theor Appl* 2000; 147(3): 267–276.
46. Chen C, Ricles JM, Sause R, et al. Experimental evaluation of an adaptive inverse compensation technique for real-time simulation of a large-scale magneto-rheological fluid damper. *Smart Mater Struct* 2010; 19: 1–12.
47. Vasilis KD, Harris PM, and Ioannis NP. On the acceleration-based adaptive inverse control of shaking tables. *Earthquake Eng Struct Dynam* 2015; 44: 1329–1350.
48. Zhang LP, Cong DC, Yang ZD, et al. Attitude synchronous tracking control of double shaking tables based on hybrid fuzzy logic cross-coupled controller and adaptive inverse controller. *J Intell Fuzzy Syst* 2015; 14: 1–10.
49. Stoten DP and Gómez EG. Adaptive control of shaking tables using the minimal control synthesis algorithm. *Phil Trans Royal Soc* 2001; 359(1786): 1697–1723.
50. Stoten DP and Shimizu N. The feedforward minimal control synthesis algorithm and its application to the control of shaking-tables. *Proc Inst Mech Eng* 2007; 221(3): 423–444
51. Stoten DP and Neild SA. The error-based minimal control synthesis algorithm with integral action. *Proc Inst Mech Eng* 2003; 217(3): 187–201.
52. Neild SA, Drury D, and Stoten DP. An improved substructuring control strategy based on the adaptive minimal control synthesis control algorithm. *Proc Inst Mech Eng* 2005; 219(5): 305–317.
53. Gizatullin AO and Edge KA. Adaptive control for a multi-axis hydraulic test rig. *Proc Inst Mech Eng* 2006; 221(2): 183–198.
54. Yao JJ, Fu W, Hu SH, et al. Amplitude phase control for electro-hydraulic servo system based on normalized least-mean-square adaptive filtering algorithm. *J Cent South Univ Technol* 2011; 18(3): 755–759.
55. Yao JJ, Hu SH, Fu W, et al. Harmonic cancellation for electro-hydraulic servo shaking table based on LMS adaptive algorithm. *J Vib Contr* 2011; 17(12): 1862–1868.
56. Yao JJ, Han Y, Xiao R, et al. Sinusoidal acceleration harmonic estimation using the extended Kalman filter for an electro-hydraulic servo shaking table. *J Vib Contr* 2015; 21(8): 1566–1579.
57. Ferreira JA, Gomes AF, and Quintas MR. Semi-empirical model for a hydraulic servo-solenoid valve. *Proc Inst Mech Eng* 2002; 216(3): 237–248.
58. Conte JP and Trombetti TL. Linear dynamic modeling of a uni-axial servo-hydraulic shaking table system. *Earthquake Eng Struct Dynam* 2000; 29: 1375–1404.
59. Chase JG, Hudson NH, Elliot R, et al. Non-linear shake table identification and control for near-field earthquake testing. *J Earthquake Eng* 2005; 9(4): 461–482.
60. Shotreed JS, Seible F, and Benzoni G. Simulation issues with a real-time, full-scale seismic testing system. *J Earthquake Eng* 2002; 6(1): 185–201.
61. Williams DM, Williams MS, and Blakeborough A. Numerical modeling of a servohydraulic testing system for structures. *J Eng Mech* 2001; 127(8): 816–827.
62. Zhao J, Catharine CS, and Posbergh T. Nonlinear system modeling and velocity feedback compensation for effective force testing. *J Eng Mech* 2005; 131(3): 244–253.
63. Guan GF, Wang HT, and Xiong W. Multi-input multi-output random vibration control of a multi-axis electro-hydraulic shaking table. *J Vib Contr*. Epub ahead of print 19 February 2014. DOI: http:// dx.doi.org /10.1177/1077546314521444.
64. Underwood MA and Keller T. Rectangular control of multi-shaker systems: theory and some practical results. *J Inst Environ Sci Technol* 2004; 47(1): 80–86.

65. Underwood MA and Keller T. Applying coordinate transformations to multi degree of freedom shaker control. *Sound Vibr* 2006; 40(1): 14–27.
66. Peeters B and Debille J. Multi-axial random vibration testing: a 6 degrees-of-freedom test case. In: *Proceedings of the 21st Aerospace Testing Seminar*, Manhattan Beach, California, 21–23 October 2003, pp. 47–62.
67. Guan GF, Xiong W, and Wang HT. Adaptive random control of a two-axis redundantly actuated electro-hydraulic shaking table. *J Vib Contr*. Epub ahead of print 15 December 2014. DOI: 10.1177 /1077546314563344.
68. He JF, Jiang HZ, and Tong ZZ. Modal control of a hydraulically driven redundant actuated fully parallel mechanism. *J Vib Contr* 2015 http://dx.doi.org/10.1177/10775463 15596661.
69. Yang CF and Han JW. Dynamic coupling analysis of a spatial 6-DOF electro-hydraulic parallel manipulator using a modal decoupling method. *Int J Adv Robot Syst* 2013; 10(104): 2013.
70. Wang JH, Pu JS, and Moore P. A practical control strategy for servo-pneumatic actuator systems. *Contr Eng Pract* 1999; 7: 1483–1488.
71. Ziaei K and Sepehri N. Modeling and identification of electrohydraulic servos. *Mechatronics* 2000; 10: 761–772.
72. Ioan T. Greedy sparse RLS. *IEEE Trans Signal Process* 2012; 60(5): 2194–2207.
73. Rigney BP, Pao LY, and Dale AL. Nonminimum phase adaptive inverse control for settle performance applications. *Mechatronics* 2010; 20: 35–44.
74. Zhao JS, Shen G, and Han JW. Feel force control incorporating velocity feed-forward and inverse model observer for control loading system of flight simulator. *Proc Inst Mech Eng* 2012; 227(2): 161–175.
75. Zhao JS, Shen G, Zhu WD, et al. Force tracking control of an electro-hydraulic control loading system on a flight simulator using inverse model control and a damping compensator. *Trans Inst Meas Contr*. Epub ahead of print 10 June 2016. DOI: 10:0142331216651326.
76. Sharq M. Internal control structure using adaptive inverse control strategy. *ISA Trans* 2005; 44(3): 353–362.
77. Qian YL, Ou G, Maghareh A, et al. Parametric identification of a servo-hydraulic actuator for real-time hybrid simulation. *Mech Syst Signal Process* 2014; 48(1–2): 260–273.
78. Mohanty A and Yao B. Indirect adaptive robust control of hydraulic manipulators with accurate parameter estimates. *IEEE Trans Contr Syst Technol* 2011; 19(3): 567–575.
79. Ozcelik O, Luco JE, and Conte JP. Experimental characterization, modeling and identification of the NEES-UCSD shake table mechanical system. *Earthquake Eng Struct Dynam* 2008; 37: 243–264.
80. Luh GC and Wu CY. Inversion control of non-linear systems with an inverse NARX model identified using genetic algorithms. *Proc Inst Mech Eng* 2000; 214(4): 259–271.
81. Rigney BP, Pao LY, and Dale AL. Discrete-time exact and approximate dynamic inversion for settle performance. In: *Proceedings of the 17th IFAC World Congress*, 2008, pp. 1778–1784.
82. Rigney BP, Pao LY, and Dale A. Nonminimum phase dynamic inversion for settle time applications. *IEEE Trans Contr Syst Technol* 2009; 17(5): 989–1005.
83. Butterworth JA, Pao LY, and Abramovitch DY. Analysis and comparison of three discrete-time feedforward model-inverse control techniques for nonminimum-phase systems. *Mechatronics* 2012; 22: 577–587.
84. Karer G, Mušič G, and Igor Š. Feedforward control of a class of hybrid systems using an inverse model. *Math Comput Simul* 2011; 82: 414–427.
85. Della LF and Gründling HA. Time domain sinusoidal acceleration controller for an electrodynamic shaker. *IET Contr Theor Appl* 2008; 2(12): 1044–1053.
86. Tang Y, Zhu ZC, Shen G, et al. Improved feedforward inverse control with adaptive refinement for acceleration tracking of electro-hydraulic shake table. *J Vibr Contr*. Epub ahead of print 29 January 2015. DOI:10.1177/ 1077546314567725.
87. Zhao JS, Shen G, Zhu WD, et al. Robust force control with a feed-forward inverse model controller for electro-hydraulic control loading systems of flight simulators. *Mechatronics* 2016; 38: 42–53. DOI: org/10.1016/j.mechatronics.
88. Pipeleers G and Swevers J. Optimal feedforward controller design for periodic inputs. *Int J Contr* 2010; 83(5): 1044–1053.
89. Shen G, Lv GM, Cong DC, et al. Feed-forward inverse control for transient waveform replication on electro-hydraulic shaking table. *J Vibr Contr* 2012; 18(10): 1474–1493.
90. MTS Systems Corporation, Eden Prairie, Minnesota, USA. Aerospace testing solutions, 2011, https://www.mts.com/ucm/groups/public/documents/library/dev_002322.pdf.
91. Hertrampf B and Mladek V. The ITFC control with an MBS Truck Test rig, 2007, Munich, Germany, http://www.simpack.com/uploads/media/um07_man_hertrampf_09.pdf
92. Stroud RC, Hamma GA, Underwood MA, et al. A review of multiaxis/multiexciter vibration technology. *Sound Vibr* 1996; 30(4): 20–27.
93. Yang ZD, Huang QT, Han JW, et al. Adaptive inverse control of random vibration based on the filtered-X LMS algorithm. *Earthquake Eng Eng Vibr* 2010; 9(1): 141–146.
94. Underwood MA and Keller T. Recent system developments for multi-actuator vibration control. *Sound Vibr* 2001; 35(10): 16–23.
95. Widrow B and Walach E. *Adaptive inverse control*. Hoboken, New York: Wiley-IEEE Press; 2008.
96. Salehzadeh-Nobari S, Chambers JA, and Green TC. Implementation of frequency domain adaptive control in vibration test products. *In:* 5th International Conference on FACTORY, Cambridge, 2–4 April 1997, 2000; pp. 264–268.
97. Stoten DP and Benchoubane H. Empirical studies of a MRAC algorithm with minimal controller synthesis. *Int J Contr* 1990; 51(4): 823–849.
98. August K and Daniel VG. On the use of a priori knowledge in adaptive inverse control. *IEEE Trans Circ Syst* 2000; 47(1): 54–62.

99. Michael AV, William TB, and William RS. Stability and operating constraints of adaptive LMS-based feedback control. *Automatica* 2003; 39: 595–605.
100. Morgan DR. An analysis of multiple correlation cancellation loops with a filter in the auxiliary path. *IEEE Trans Acoust Speech Signal Process* 1980; 28(4): 454–467.
101. Lin C and Chen P. Precision tracking control of a biaxial piezo stage using repetitive control and double-feedforward compensation. *Mechatronics* 2011; 21: 239–249.
102. Ahmadizadeh M, Mosqueda G, and Reinhorn AM. Compensation of actuator delay and dynamics for real-time hybrid structural simulation. *Earthquake Eng Struct Dynam* 2011; 37(1): 21–42.
103. Horiuchi T, Inoue M, Konno T, et al. Real-time hybrid experimental system with actuator delay compensation and its application to a piping system with energy absorber. *Earthquake Eng Struct Dynam* 1999; 28(10): 1121–1141.
104. Chen C and Ricles JM. Large-scale real-time hybrid simulation involving multiple experimental substructures using an adaptive actuator delay compensation method. *Earthquake Eng Struct Dynam* 2012; 41(3): 549–569.
105. Horiuchi T and Konnno T. A new method for compensation actuator delay in real-time hybrid experiment. *Phil Trans Roy Soc Lond A* 2001; 359(1786): 1893–1909.
106. Mahnaz H. Adaptive control for a class of MIMO nonlinear time delay systems against time varying actuator failures. *ISA Trans* 2015; 57: 23–42.
107. Wang YJ. Characterization and quenching of friction-induced limit cycles of electro-hydraulic servovalve control systems with transport delay. *ISA Trans* 2010; 49: 489–500.